

LHC Effective Model for Optics Corrections

Maël Le Garrec

CERN, March 21, 2024

Temporary Plan

- b5 studies
 - DA simulations
 - * Knobs created via resp matrix
 - * Knobs tested via MADX with rdt tunes
 - * Same knob re-tested with OP tunes
 - * How is DA computed?

Check yourself before you Shrek yourself.

ICE CUBE FT. SHREK

Abstract

Zusammenfassung

Acknowledgements

Contents

Abstract	v
Zusammenfassung	vii
Acknowledgements	ix
Contents	x
Glossary	xv
1. Introduction	1
1.1. Motivation	2
1.2. Thesis Outline	2
1.3. Particle Accelerators and CERN	2
1.3.1. Particle Accelerators	2
1.3.2. The CERN Complex	3
1.3.3. The Large Hadron Collider	4

2. Concepts of Accelerator Physics	7
2.1. Introduction	9
2.2. Magnetic Fields	9
2.2.1. Nomenclature	9
2.2.2. Multipole Expansion	10
2.2.3. Beam Rigidity and Normalization	11
2.2.4. Hamiltonian Dynamics	12
2.3. Coordinate Systems	12
2.3.1. Frenet-Serret System	12
2.3.2. Linear Lattice	13
2.3.3. Non-Linear Lattice	16
2.4. Beam Observables	19
2.4.1. Dispersion	19
2.4.2. β-function	20
2.4.3. Coupling	21
2.4.4. Momentum Compaction Factor	21
2.5. Detuning Effects	21
2.5.1. Chromaticity	22
2.5.2. Amplitude Detuning	25
2.5.3. Chromatic Amplitude Detuning	26
2.6. Resonances	27
3. Optics Measurements and Corrections	29
3.1. Beam Instrumentation	30
3.1.1. Beam Position Monitors	30
3.1.2. Beam Loss Monitors	31
3.1.3. AC-Dipole	31
3.2. Optics Measurements	32
3.2.1. Turn by Turn	32
3.2.2. Chromaticity	32
3.3. Correction Principles	35
3.3.1. Response Matrix	35

3.3.2. Chromaticity	37
4. Decapole Measurements, Corrections and Modelling in the LHC	39
4.1. Motivation	40
4.2. Non-Linear Chromaticity	41
4.3. Chromatic Amplitude Detuning	41
4.4. Resonance Driving Terms	41
4.4.1. Decapolar Contribution	42
4.4.2. Lower Order Contributions	42
4.5. Impact of Decapolar Fields	42
4.6. Integrating Decay	42
5. Very High Order Field Measurement in the LHC	43
5.1. First Measurement of Fourth and Fifth Order Chromaticity	44
5.2. INTRODUCTION	44
5.3. NL-CHROMATICITY MEASUREMENTS	45
5.3.1. Nominal Corrections	45
5.3.2. Beam-Based Corrections	47
5.3.3. $Q^{(4)}$ and $Q^{(5)}$ fit quality	48
5.4. NL-CHROMATICITY MODEL	50
5.5. CONCLUSIONS AND OUTLOOK	51
5.6. First Measurement of Dodecapole RDTs	52
6. Skew Octupole Fields in the LHC	55
6.1. Correction of skew octupole Fields at Top Energy	56
6.2. Correction of Skew Octupole Fields at Injection Energy	56
6.3. Skew Octupolar Fields from Landau Octupoles	57
A. Units and Conversions	59
A.1. Physical Constants	59
A.2. Units	59
A.3. Conversions	59

Contents

B. Resonance Driving Terms	61
B.1. Frequency Spectrum Lines	62
B.1.1. Horizontal Axis	62
B.1.2. Vertical Axis	64
B.2. Amplitude, Resonances and Lines	67
Bibliography	75
List of Publications	79

Glossary

Nomenclature

AC-Dipole Dipole magnet generating a variable oscillating field. Used to force beam oscillations for optics measurements. .

Aperture Maximum physical transverse size the beam can take in the accelerator without suffering losses.

ATS Factor Equivalent to the ratio of the virgin β -function to the β -function used in the current ATS scheme, at the edge of the arc.

Beta-function Variable of the twiss-parameters: β as a function of the longitudinal position s . Related to the transverse beam size: $\sigma(s) = \sqrt{\epsilon \cdot \beta(s)}$

.

BPM Beam Position Monitor, gives the transverse position of the beam.

Chromaticity Tune change with momentum offset. Usually denoted as three orders: Q' , Q'' and Q''' .

Coupling Correlation between the motion of particles in horizontal or vertical plane to the other. Strong coupling negatively impacts the optics and is usually avoided. .

Glossary

Crosstalk Interferences between two electronic circuits.

Dipole Magnets with two poles, responsible for bending the particles in the accelerator..

Dispersion Change of orbit with momentum offset, mainly in the horizontal plane, created by the dipoles.

DOROS Low noise BPM. Currently can't be used with other BPMs due to synchronization issues.

Dynamic Aperture Maximum stable aperture. Above that size, the particles become unstable and become lost.

Emittance (ϵ) Unit describing the beam in phase space. A low emittance indicates a beam with a small momentum offset and confined to a small distance.

Laundau Octupole Octupoles that introduce a spread in the beam, making it more stable.

LBDS LHC Beam Dump System.

Orbit Feedback System responsible for acquisition and correction of the orbit.

Rigid Waist Shift Doing a waist shift by powering all the triplets at once. No individual trim.

Waist Location where the β -function is at its minimum in an IP. β^* refers to β_{waist} .

Waist Shift Changing the waist to have $\beta^* = \beta_{IP}$.

Acronyms

LHC Large Hadron Collider.

Symbols

action Action used as coordinate blabla.

1

Introduction

Contents

1.1.	Motivation	2
1.2.	Thesis Outline	2
1.3.	Particle Accelerators and CERN	2
1.3.1.	Particle Accelerators	2
1.3.2.	The CERN Complex	3
1.3.3.	The Large Hadron Collider	4

1. Introduction

1.1. Motivation

1.2. Thesis Outline

1.3. Particle Accelerators and CERN

1.3.1. Particle Accelerators

GPT

The history of particle accelerators is a captivating narrative that spans over a century of scientific innovation and discovery. It is a journey that has fundamentally transformed our understanding of the universe's fundamental particles and their interactions. The concept of accelerating particles to high speeds originated in the late 19th century, with early experiments conducted by pioneers such as J.J. Thomson and Ernest Rutherford, who utilized basic devices like cathode ray tubes to propel electrons.

One of the earliest breakthroughs in accelerator technology was the Cockcroft-Walton accelerator, introduced in 1932 by John Cockcroft and Ernest Walton. This pioneering device employed voltage multipliers to accelerate protons and ions, enabling the first artificial nuclear disintegration—a milestone that earned them the Nobel Prize in Physics in 1951. Building upon this achievement, the development of the synchrotron in the 1940s and 1950s by scientists like Edwin McMillan and Vladimir Veksler marked a significant stride. Synchrotrons harnessed magnetic fields to bend and accelerate charged particles in circular paths, advancing the study of particle properties.

A key turning point emerged with the establishment of CERN (the European Organization for Nuclear Research) in 1954, which culminated in the creation of the Proton Synchrotron (PS) in 1959. This marked the emergence of a powerful era in accelerator science, enabling the discovery of novel particles and laying the groundwork for the formulation of the Standard Model of particle physics.

Throughout the 1960s and 1970s, the advent of bubble chambers and bubble chamber detectors provided researchers with the ability to trace the paths of charged particles, leading to the revelation of various particles and their intricate interactions.

Yet, the true marvel of accelerator technology came to the forefront with the construction of the Large Hadron Collider (LHC) at CERN, which commenced operation in 2008. The LHC, an awe-inspiring 27-kilometer ring of superconducting magnets, propels protons and heavy ions to velocities nearing the speed of light. The LHC's monumental achievement—the discovery of the Higgs boson in 2012—marked a crowning moment in particle physics, solidifying the vital role of particle accelerators in unraveling the fabric of the cosmos.

As particle physicists peer into the future, the quest continues. Concepts such as linear colliders and advanced circular colliders are on the horizon, promising to delve even deeper into the enigmatic realm of fundamental particles and the forces that govern them. The history of particle accelerators underscores the profound human endeavor to explore the most intricate mysteries of the universe, revealing the intricate dance of particles that shape the cosmos and expanding the horizons of human knowledge.

1.3.2. The CERN Complex

GPT The CERN complex, located near Geneva, Switzerland, is a prominent center for particle physics research. Its centerpiece is the Large Hadron Collider (LHC), the world's largest particle accelerator with a 27-kilometer circumference. Here, protons and heavy ions are accelerated to near light speed and collide at various points for fundamental particle studies. Surrounding the LHC are significant particle detectors, including ATLAS, CMS, ALICE, and LHCb, designed to capture and analyze particles generated during these collisions.

CERN also includes linear accelerators, the Proton Synchrotron (PS), Super Proton Synchrotron (SPS), and Antiproton Decelerator (AD), contributing to

1. Introduction

particle acceleration and antimatter research. Alongside these facilities, CERN houses the Theoretical Physics Department, where theorists collaborate with experimentalists. With research, administrative buildings, laboratories, and workshops, CERN provides a comprehensive environment for scientific exploration. Its history, including the 2012 discovery of the Higgs boson, underscores its importance in advancing particle physics and highlighting international scientific cooperation.

1.3.3. The Large Hadron Collider



Figure 1.1.: 3D cut of a main LHC dipole [1].

speed of light, 11 000 turns per second, 12 000 amps in dipoles, number dipoles, price, parameters energy consumption, detectors and experiments, discoveries,

collimators, optics, magnets, luminosity, arcs, IRs, schematics, cryostat, beta function FODO

1. Cycles & types of bunches: pilot for measurements

2

Concepts of Accelerator Physics

Contents

2.1.	Introduction	9
2.2.	Magnetic Fields	9
2.2.1.	Nomenclature	9
2.2.2.	Multipole Expansion	10
2.2.3.	Beam Rigidity and Normalization	11
	Beam Rigidity	11
	Field Normalization	11
2.2.4.	Hamiltonian Dynamics	12
2.3.	Coordinate Systems	12
2.3.1.	Frenet-Serret System	12
2.3.2.	Linear Lattice	13
	Courant-Snyder Parameters	13
	Linear Transfer Map	16

2. Concepts of Accelerator Physics

2.3.3.	Non-Linear Lattice	16
	Lie Algenra	16
	Poisson Brackets	17
	Lie Operator	17
	Non-Linear Transfer Maps	18
	Normal Form	19
2.4.	Beam Observables	19
2.4.1.	Dispersion	19
2.4.2.	β -function	20
2.4.3.	Coupling	21
2.4.4.	Momentum Compaction Factor	21
2.5.	Detuning Effects	21
2.5.1.	Chromaticity	22
	Natural Chromaticity from Quadrupoles	22
	Linear Chromaticity from Sextupoles	23
	Non-Linear Chromaticity	25
2.5.2.	Amplitude Detuning	25
2.5.3.	Chromatic Amplitude Detuning	26
2.6.	Resonances	27

1. Coordinates
 - a) Linear Maps
 - b) Normal Form & RDT & resonance diagram
2. Chromaticity
 - a) Combined effect of multipoles
 - b) Amplitude Detuning
 - c) Chromtic Amplitude Detuning
 - d) Dynamic Aperture
3. Luminosity

2

2.1. Introduction

2.2. Magnetic Fields

2.2.1. Nomenclature

Several notations coexist to denote magnetic fields. In this thesis, the *European Convention* [2] is used for field indices, as shown in Tab. 2.1. MAD-X, and MAD-NG, however, use the *American Convention*.

Multipole	MAD-X	Index	Normalized Strength
Dipole	0	1	K_1
Quadrupole	1	2	K_2
Sextupole	2	3	K_3
Octupole	3	4	K_4
Decapole	4	5	K_5
Dodecapole	5	6	K_6
Decatetrapole	6	7	K_7

Table 2.1.: Relation between field indices and multipoles.

As such, unless explicitly stated, quantities such as the magnetic strength b and normalized strength K will be expressed with this notation.

2.2.2. Multipole Expansion

A 2 dimension magnetic field in the planes x and y can be described as a sum of the normal and skew field gradients \mathcal{B} and \mathcal{A} with multipoles of order n , given by [3]:

$$B_y + iB_x = \sum_{n=1}^{\infty} (\mathcal{B}_n + i\mathcal{A}_n) (x + iy)^{n-1} \quad (2.1)$$

An ideal magnet would produce either a sole normal or skew field. However, this is not applicable to real-life magnets that are imperfect, due to design and manufacturing constraints. Field errors are thus introduced, relative to the main field of the ideal 2N-pole magnet at a reference radius r_{ref} [2], as shown in Eq. (2.2). The coefficients of the normal and skew relative field errors, referred to as a_n and b_n , are dimensionless but often given in *units* of 10^{-4} .

$$B_y + iB_x = \begin{cases} \mathcal{B}_N \cdot \sum_{n=1}^{\infty} (b_n + ia_n) \left(\frac{x+iy}{r_{ref}}\right)^{n-1}, & \text{for normal magnets} \\ \mathcal{A}_N \cdot \sum_{n=1}^{\infty} (b_n + ia_n) \left(\frac{x+iy}{r_{ref}}\right)^{n-1}, & \text{for skew magnets} \end{cases} \quad (2.2)$$

The normal and skew field components of order n for an imperfect 2N-pole magnet is thus given by the following equation:

$$\begin{aligned} \mathcal{B}_n &= \mathcal{B}_N \cdot \frac{b_n}{r_{ref}^{n-1}}, \\ \mathcal{A}_n &= \mathcal{A}_N \cdot \frac{a_n}{r_{ref}^{n-1}}. \end{aligned} \quad (2.3)$$

The unit of the field is relative to the multipole order n : [Tm $^{1-n}$].

2.2.3. Beam Rigidity and Normalization

Beam Rigidity

The beam rigidity refers to the resistance of a particle moving through the accelerator to the bending applied by the magnetic fields. It is derived from the Laurentz force [2] and relates the magnetic field B , the radius of curvature ρ to the momentum p and charge q of the particle:

$$B\rho = \frac{p}{q} \quad (2.4)$$

It is of interest when designing an accelerator to set the maximum field as well as the required radius of curvature for a specific momentum and particle. An interesting metric of an accelerator is also its *filling factor*, or percentage of dipoles in the machine. It can be calculated via the radius of curvature: $f = \rho/r$. A low filling factors means more space for other magnets, collimators, beam instrumentation, etc.

Field Normalization

The Beam Rigidity is also used as a way to normalize magnetic field strengths in particle accelerators where the momentum of the particle changes (i.e. acceleration). Normalized Normal and Skew components K_n and J_n are given by [3]:

$$\begin{aligned} K_n &= \frac{q}{p}(n-1)!\mathcal{B}_n, \\ J_n &= \frac{q}{p}(n-1)!\mathcal{A}_n. \end{aligned} \quad (2.5)$$

2. Concepts of Accelerator Physics

2.2.4. Hamiltonian Dynamics

The Hamiltonian describing the motion for the transverse planes of a given multipole or order n is given by [4–6]:

$$\begin{aligned} H &= \frac{q}{p} \Re \left[\sum_{n>1} (\mathcal{B}_n + i\mathcal{A}_n) \frac{(x+iy)^n}{n} \right] \\ &= \Re \left[\sum_{n>1} (K_n + iJ_n) \frac{(x+iy)^n}{n!} \right]. \end{aligned} \quad (2.6)$$

Quite often, when studying the effect of a magnet on the beam, only one component is required, and the sum can thus be dropped. The normal and skew fields can also be isolated in order to consider their effect only:

$$\begin{aligned} N_n &= \frac{1}{n!} K_n \Re [(x+iy)^n] \\ S_n &= -\frac{1}{n!} J_n \Im [(x+iy)^n]. \end{aligned} \quad (2.7)$$

2.3. Coordinate Systems

In circular accelerators, particle dynamics are represented using a traveling coordinate system. A reference orbit is determined by the lattice and its magnet strengths, forming the *optics*. In the case of a synchrotron, like the LHC, where the particles return to their original location after some turns, the reference orbit is also called the closed orbit.

2.3.1. Frenet-Serret System

The Frenet-Serret coordinate system moves along the ring on the reference orbit. The coordinates are then transverse: x and y , and longitudinal in the direction of travel: s . Figure 2.1 shows those coordinates.

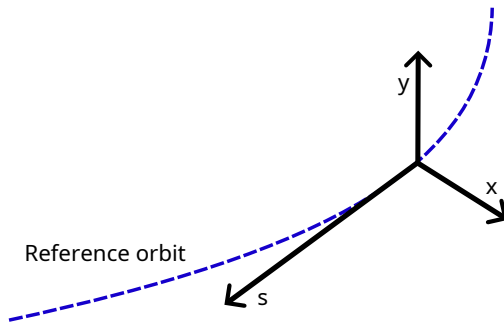


Figure 2.1.: Frenet-Serret coordinate system, commonly used in accelerator physics. The system moves along the reference orbit.

This coordinate system is widely used to simply describe either an element's or a particle's position in the accelerator. Without any explicit mention, those are coordinates used in this thesis. It is frequent to use the variable z to refer to either x or y in equations.

2.3.2. Linear Lattice

Courant-Snyder Parameters

A circular accelerator is composed of many multipoles of different orders. A basic design only requires dipoles and quadrupoles in order to operate. Dipoles are used to bend the particles in order to form the ring, whereas quadrupoles are used to focus the beam to a focal point, similar to light optics. Those elements can be arranged in a particular order, to form a FODO cell. Such cells present an alternating placement of focusing and defocusing quadrupoles with dipoles in between, as shown in Fig.2.2, and are usually repeated many times along the ring.

2. Concepts of Accelerator Physics

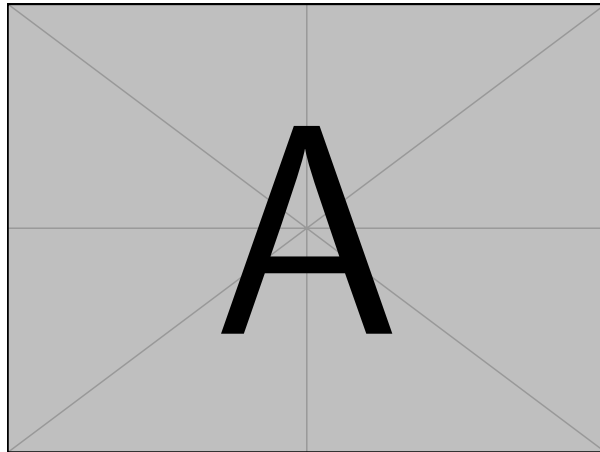


Figure 2.2.: **FODO cell, a repeated basic block present in most circular accelerators.**

A lattice composed of only dipoles and quadrupoles, is referred to as a *linear* lattice. In a synchrotron, a circular particle accelerator, particles undergo transverse and longitudinal oscillations. As such, particles do not go back to their initial position before a certain number of turns. Taking into account those oscillations, the phase-space ellipse of a particle at a position s in the ring can be described with a new system: the Courant-Snyder parameters, also known as Twiss parameters or the *optics functions* [7], as shown in Fig. 2.3.

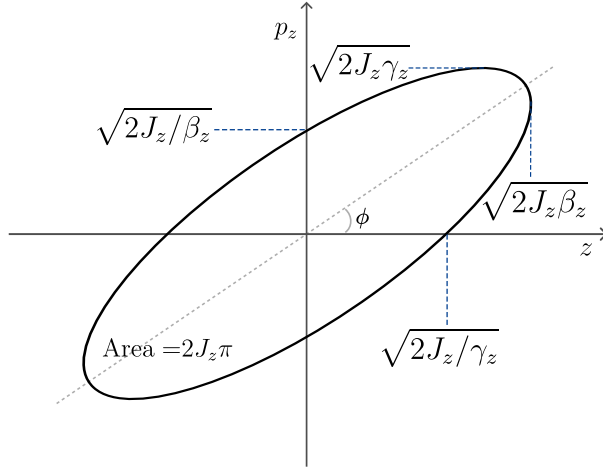


Figure 2.3.: Phase-space ellipse of a linear machine, parametrized by the Courant-Snyder parameters α , β and γ .

J , the action, an invariant of motion at a given energy, is related to the other quantities by:

$$J_z = \frac{1}{2}(\gamma_z \cdot z^2 + 2\alpha_z p_z \cdot z + \beta_z p_z^2). \quad (2.8)$$

The action can be related to the area in phase space, called the emittance: $\epsilon = 2J$. As the β parameter varies along the ring, it is referred to as the β -function and is related to the amplitude of the oscillations. Thus, the smaller is the β -function, the smaller is also the envelope of the beam. The number of oscillations per turn is called the *tune*, and is closely related to the β -function:

$$Q_{x,y} = \frac{1}{2\pi} \oint \frac{1}{\beta_{x,y}(s)} ds. \quad (2.9)$$

It is common to express the position of a particle using *action-angle* variables, allowing to switch between the Courant-Snyder parameters and the Frenet-Serret

2. Concepts of Accelerator Physics

system:

$$\begin{aligned} z &= \sqrt{2J_z\beta_z} \cos \phi_z \\ p_z &= -\sqrt{\frac{2J_z}{\beta_z}} (\sin \phi_z + \alpha_z \cos \phi_z). \end{aligned} \quad (2.10)$$

Linear Transfer Map

2.3.3. Non-Linear Lattice

Lie Algebra

So far, Courant-Snyder parameters were a good way to describe the distribution of positions and velocities of particles in the transverse plane. One caveat of using this formalism is that it is restrained to linear optics and does not describe non-linear beam dynamics such as resonances or the effects arising from an arrangement of several multipoles together.

One way to describe such effects is to introduce Lie Algebra [8], a vector space \mathfrak{g} equipped with a binary operation called the *Lie bracket* and denoted $[x, y]$ for two vectors x and y . Any vector space equipped with a Lie bracket (or multiplication rule) satisfying the following conditions is called a Lie algebra:

- Bilinearity:

$$\begin{aligned} [ax + by, z] &= a[x, z] + b[y, z], \\ [z, ax + by] &= a[z, x] + b[z, y], \quad \forall x, y, z \in \mathfrak{g} \text{ and } a, b \text{ scalars} \end{aligned} \quad (2.11)$$

- Alternativity:

$$[x, x] = 0, \quad \forall x \in \mathfrak{g} \quad (2.12)$$

- Anticommutativity:

$$[x, y] = -[y, x], \quad \forall x, y \in \mathfrak{g} \quad (2.13)$$

- The Jacobi identity:

$$[x, [y, z]] + [y, [z, x]] + [z, [x, y]] = 0, \quad \forall x, y, z \in \mathfrak{g} \quad (2.14)$$

Poisson Brackets

To create a Lie algebra, an operation satisfying those conditions needs to be found. In accelerator physics, *Poisson brackets* are chosen [8, 9]. Let's consider position and momentum coordinates $q_i \cdots q_n$ and $p_i \cdots p_n$ of a $2n$ -dimensional phase space. Usually, those would be x, y, p_x and p_y for transverse coordinates. The Poisson brackets of two functions f and g if then defined by:

$$[f, g] = \sum_{i=1}^n \frac{\partial f}{\partial q_i} \frac{\partial g}{\partial p_i} - \frac{\partial f}{\partial p_i} \frac{\partial g}{\partial q_i}. \quad (2.15)$$

Lie Operator

Given a function f , a differential operator called *Lie operator* is defined, and is closely related to the previously seen Poisson bracket:

$$\mathcal{L}_f := \sum_{i=1}^n \frac{\partial f}{\partial q_i} \frac{\partial}{\partial p_i} - \frac{\partial f}{\partial p_i} \frac{\partial}{\partial q_i}. \quad (2.16)$$

The action of this operator on a function g is equivalent to the Poisson brackets, as in:

$$\mathcal{L}_f g = [f, g]. \quad (2.17)$$

A particular power series of this Lie operator can now be defined, called *Lie transformation*:

$$\begin{aligned} e^{[f]} g &= \sum_{l=0}^{\infty} \frac{1}{l!} : f :^l g \\ &= g + [f, g] + \frac{1}{2!} [f, [f, g]] + \dots \end{aligned} \quad (2.18)$$

Non-Linear Transfer Maps

As introduced **before**, the dynamics of a particle beam in a circular accelerator can be described by *transfer maps*. A symplectic *One Turn Map* \mathcal{M} that also includes N non-linear elements is defined [8] as:

$$\mathcal{M} = e^{[h_N]} \cdot e^{[h_{N-1}]} \cdots e^{[h_1]} \cdot \mathcal{R} \quad (2.19)$$

where \mathcal{R} is a matrix describing the linear motion over one turn and the h_i terms representing the Hamiltonian of each non-linear elements of the machine. Via the Baker-Campbell-Hausdorff (BCH) **citation** theorem, previous Lie transformations can be combined and simplified:

$$e^{[h_1]} \cdot e^{[h_2]} = e^{[h]} \quad (2.20)$$

with

$$\begin{aligned} h &= h_1 + h_2 \\ &\quad + \frac{1}{2} [h_1, h_2] \\ &\quad + \frac{1}{12} [h_1, [h_1, h_2]] - \frac{1}{12} [h_2, [h_1, h_2]] + \dots \end{aligned} \quad (2.21)$$

The one turn map is thus expressed as a single Lie transformation:

$$\mathcal{M} = e^{[h]} \cdot \mathcal{R}. \quad (2.22)$$

In most cases, were the non-linear perturbations are small, the above series converges quickly and only the two first terms of Eq. (2.21) are used [10]. The resulting expression is then more elegant, being a simple sum of the Hamiltonians of the N non-linear elements:

$$\mathcal{M} = e^{:h_1+h_2+\dots+h_N:} \cdot \mathcal{R}. \quad (2.23)$$

It is though to be noted that in this thesis experimental measurements show the evidence of higher order contributions. In order to fully understand the combined effect of multipoles, the BCH expansion needs to be expended further than the first two terms.

Normal Form

2.4. Beam Observables

title?

Linear observables

Optics

2.4.1. Dispersion

Treating a beam as a single particle having the design momentum p_0 leads to a machine with no apparent ill effect related to that momentum. However, when considering a particle beam where each particle follows a distribution in momentum, a few effects arise from this deviation, called the *momentum offset*, δ . It is defined as a relative difference to the design momentum:

$$\delta = \frac{p - p_0}{p_0}. \quad (2.24)$$

2. Concepts of Accelerator Physics

Those effects are referred to as *chromatic aberrations*. The first and most important to consider is the *dispersion*. Dispersion results from a particle with a momentum offset being deflected differently by the dipoles compared to a particle at the design momentum. Figure 2.4 shows an example of deflection.

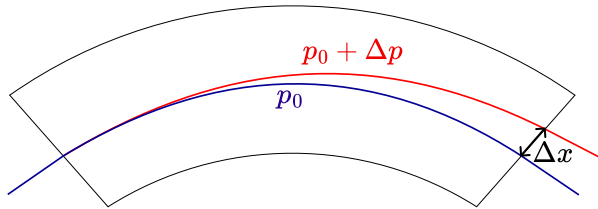


Figure 2.4.: Particles with a momentum offset will be deflected differently by dipoles. This offset in position can be described by the dispersion function.

The particle is still subject to the other properties of the lattice, but with a different orbit, described by Eq. (2.4).

$$\begin{aligned} D_x(s) &= \frac{\Delta x(s)}{\delta} \\ D_y(s) &= \frac{\Delta y(s)}{\delta} \end{aligned} \tag{2.25}$$

2.4.2. β -function

As seen previously in 2.3.2, the β -function is related to the amplitude of oscillations of the beam. Figure 2.5 shows how the β -function oscillates along the ring due to quadrupoles focusing and defocusing properties. The β -function is an important quantity found as a factor in several other observables that will be described later in this thesis.

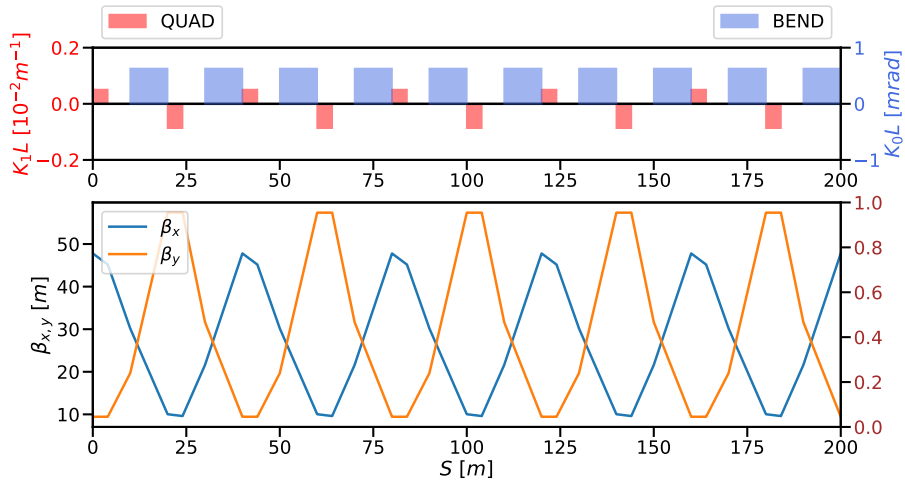


Figure 2.5.: Evolution of the β -function along the lattice. Horizontal and vertical beatings are usually opposite given the focusing and defocusing properties of quadrupoles in each plane.

A difference in β -function compared to the design leads to possible unstable and larger beams, degrading its properties and making it harder to control. The relative difference in β -function is called the beta-beating, expressed in percents:

$$\text{beating [\%]} = \frac{\beta_z(s) - \beta_z(s)_{model}}{\beta_z(s)_{model}}. \quad (2.26)$$

2.4.3. Coupling

2.4.4. Momentum Compaction Factor

2.5. Detuning Effects

blabla

2. Concepts of Accelerator Physics

2.5.1. Chromaticity

Chromaticity is the tune change ΔQ relative to the momentum offset δ . Chromaticity can be described by a Taylor expansion, given by

$$Q(\delta) = Q_0 + Q'\delta + \frac{1}{2!}Q''\delta^2 + \frac{1}{3!}Q'''\delta^3 + \mathcal{O}(\delta^4). \quad (2.27)$$

Or, more generally, rewritten as a sum to include all orders up to n :

$$Q(\delta) = Q_0 + \sum_{i=1}^n \frac{1}{i!} Q^{(i)} \delta^i. \quad (2.28)$$

The first order of the chromaticity expansion, Q' , is generally simply referred to as *chromaticity*, sometimes as *linear chromaticity*. The other terms are thus referred to as *non-linear chromaticity*.

The chromaticity change induced by a single element of order n and length L can be derived from the Hamiltonian of Eq. (2.6), averaging over the phase variables and differentiating relative to the actions $J_{x,y}$ and the momentum offset δ :

$$\Delta Q_{x,y}^{(n)} = \frac{\partial^n Q_{x,y}}{\partial^n \delta} = \frac{1}{2\pi} \int_L \left\langle \frac{\partial^{(n+1)} H}{\partial J_{x,y} \partial^n \delta} \right\rangle ds. \quad (2.29)$$

Natural Chromaticity from Quadrupoles

In a purely linear lattice, the linear chromaticity, Q' , is a result of the momentum dependence of the quadrupoles' focusing. It is in this case called the *natural chromaticity* and can be derived from the normal hamiltonian of Eq.(2.7) and expressing the normalized magnet strength K with a dependence on δ via P as $P_0(1 + \delta)$:

$$K_n = \frac{q}{P_0} \frac{1}{1+\delta} (n-1)! B_n \quad (2.30)$$

The normal field of a quadrupole is then given by

$$\mathcal{N}_2(x, y) = \frac{1}{2} \frac{q}{P_0} \frac{1}{1+\delta} B_2 (x^2 - y^2) \quad (2.31)$$

By operating a variable change to the angle coordinates ($x \rightarrow \sqrt{2J_x\beta_x} \cos \phi_x$ and $y \rightarrow \sqrt{2J_y\beta_y} \cos \phi_y$), the following equation linking the β -function and δ to the normal field is obtained:

$$\mathcal{N}_2(x, y) = \frac{1}{2} \frac{q}{P_0} \frac{1}{1+\delta} B_2 \left[\left(\sqrt{2J_x\beta_x} \cos \phi_x \right)^2 - \left(\sqrt{2J_y\beta_y} \cos \phi_y \right)^2 \right]. \quad (2.32)$$

Following Eq.(2.29), the natural chromaticity Q' induced by quadrupoles is given by:

$$\begin{aligned} \Delta Q'_x &= \frac{1}{2\pi} \int_L \frac{\partial^2 \langle \mathcal{N}_2 \rangle}{\partial J_x \partial \delta} ds \quad ; \quad \Delta Q'_y &= \frac{1}{2\pi} \int_L \frac{\partial^2 \langle \mathcal{N}_2 \rangle}{\partial J_y \partial \delta} ds \\ &= -\frac{1}{4\pi} \frac{q}{P_0} B_2 L \beta_x && = \frac{1}{4\pi} \frac{q}{P_0} B_2 L \beta_y \end{aligned} \quad (2.33)$$

Linear Chromaticity from Sextupoles

The first order chromaticity Q' is contributed to by sextupoles in the presence of off-momentum particles. The normal field of a sextupole, following Eq.(2.7) is given by

$$\mathcal{N}_3(x, y) = \frac{1}{3!} (x^3 - 3xy^2). \quad (2.34)$$

As the momentum offset δ introduces a change in orbit via dispersion [11], a variable change can be operated on both x and y , as shown in Eq.(2.35). In

this thesis, vertical dispersion will be though neglected.

$$\begin{aligned} x &\rightarrow x + \Delta x = x + D_x \delta \\ y &\rightarrow y + \Delta y = y + D_y \delta \end{aligned} \quad (2.35)$$

The positions x and y can once be replaced, using the twiss parameters, giving the full expression:

$$\begin{aligned} \mathcal{N}_3(x + \Delta x, y) = \frac{1}{6} K_3 & \left[\left(\sqrt{2J_x\beta_x} \cos \phi_x \right)^3 \right. \\ & + 3 \left(\sqrt{2J_x\beta_x} \cos \phi_x \right)^2 D_x \delta \\ & + 3 \left(\sqrt{2J_x\beta_x} \cos \phi_x \right) D_x^2 \delta^2 \\ & + D_x^3 \delta^3 \\ & - 3 \left(\sqrt{2J_x\beta_x} \cos \phi_x \right) \left(\sqrt{2J_y\beta_y} \cos \phi_y \right)^2 \\ & \left. - 3D_x \delta (\sqrt{2J_y\beta_y} \cos \phi_y)^2 \right] \end{aligned} \quad (2.36)$$

Averaging over the phase variables removes any odd cosine:

$$\begin{aligned} \langle \mathcal{N}_3(x + \Delta x, y) \rangle = \frac{1}{6} K_3 & \left(3J_x\beta_x D_x \delta \right. \\ & + D_x^3 \delta^3 \\ & \left. - 3D_x \delta J_y \beta_y \right) \end{aligned} \quad (2.37)$$

The chromaticity can then obtained by differentiating relative to the action

$J_{x,y}$ to obtain the tune, and then by the momentum offset δ .

$$\begin{aligned}\Delta Q'_x &= \frac{1}{2\pi} \int_L \frac{\partial^2 \langle \mathcal{N}_3 \rangle}{\partial J_x \partial \delta} ds \quad ; \quad \Delta Q'_y = \frac{1}{2\pi} \int_L \frac{\partial^2 \langle \mathcal{N}_3 \rangle}{\partial J_y \partial \delta} ds \\ &= \frac{1}{2\pi} L \frac{1}{2} K_3 \beta_x D_x & &= -\frac{1}{2\pi} L \frac{1}{2} K_3 \beta_y D_x \\ &= \frac{1}{4\pi} K_3 L \beta_x D_x & &= -\frac{1}{4\pi} K_3 L \beta_y D_x\end{aligned}\quad (2.38)$$

From this last equation, it is apparent than sextupoles are not a source of chromaticity of higher orders in the presence of linear dispersion. In the presence of second order dispersion [11], sextupoles can generate some amount of Q'' , usually negligible.

Non-Linear Chromaticity

Higher orders of the chromaticity function are described in [12] and follow the same logic as for the linear chromaticity from sextupoles. A general formula can be found for the chromaticity of order $n, n > 2$:

$$\begin{aligned}\Delta Q_x^{(n)} &= \frac{1}{4\pi} K_{n+2} L \beta_x D_x \\ \Delta Q_y^{(n)} &= -\frac{1}{4\pi} K_{n+2} L \beta_y D_x\end{aligned}\quad (2.39)$$

2.5.2. Amplitude Detuning

Amplitude detuning is a tune shift induced by the amplitude of oscillations of a particle. This detuning is directly related to the emittance and can be described via a Taylor expansion. Equation (2.40) shows this expansion up to the second order. Further expansions can be found in [12].

$$Q_z(\epsilon_x, \epsilon_y) = Q_{z0} + \left(\frac{\partial Q_z}{\partial \epsilon_x} \epsilon_x + \frac{\partial Q_z}{\partial \epsilon_y} \epsilon_y \right) + \frac{1}{2!} \left(\frac{\partial^2 Q_z}{\partial \epsilon_x^2} \epsilon_x^2 + 2 \frac{\partial^2 Q_z}{\partial \epsilon_x \partial \epsilon_y} \epsilon_x \epsilon_y + \frac{\partial^2 Q_z}{\partial \epsilon_y^2} \epsilon_y^2 \right) + \dots \quad (2.40)$$

The first order terms of amplitude detuning are generated by octupoles, and to some extent by sextupoles when considering their higher order contributions. Those higher contributions are usually measurable but small compared to the ones of normal octupoles.

2.5.3. Chromatic Amplitude Detuning

Chromatic amplitude detuning is the change of tune relative to a change of amplitude *and* momentum. The tune then depends on $\epsilon_x, \epsilon_y, \delta$.

By doing a Taylor expansion (??), we can write the tune as:

$$Q_z(\epsilon_x, \epsilon_y, \delta) = Q_{z0} + \left[\frac{\partial Q_z}{\partial \epsilon_x} \epsilon_x + \frac{\partial Q_z}{\partial \epsilon_y} \epsilon_y + \frac{\partial Q_z}{\partial \delta} \delta \right] + \frac{1}{2!} \left[\frac{\partial^2 Q_z}{\partial \epsilon_x^2} \epsilon_x^2 + \frac{\partial^2 Q_z}{\partial \epsilon_y^2} \epsilon_y^2 + \frac{\partial^2 Q_z}{\partial \delta^2} \delta^2 + 2 \frac{\partial^2 Q_z}{\partial \epsilon_x \partial \epsilon_y} \epsilon_x \epsilon_y + 2 \frac{\partial^2 Q_z}{\partial \epsilon_x \partial \delta} \epsilon_x \delta + 2 \frac{\partial^2 Q_z}{\partial \delta \partial \epsilon_y} \delta \epsilon_y \right] + \dots \quad (2.41)$$

We recognise the terms in yellow, seen before: the chromaticities Q' , Q'' , and Q''' . It has been shown that only octupoles and dodecapoles contribute to the amplitude detuning. The *Chromatic* Amplitude Detuning though also adds chromatic terms, we then have to consider more multipoles.

make it clear I derived it

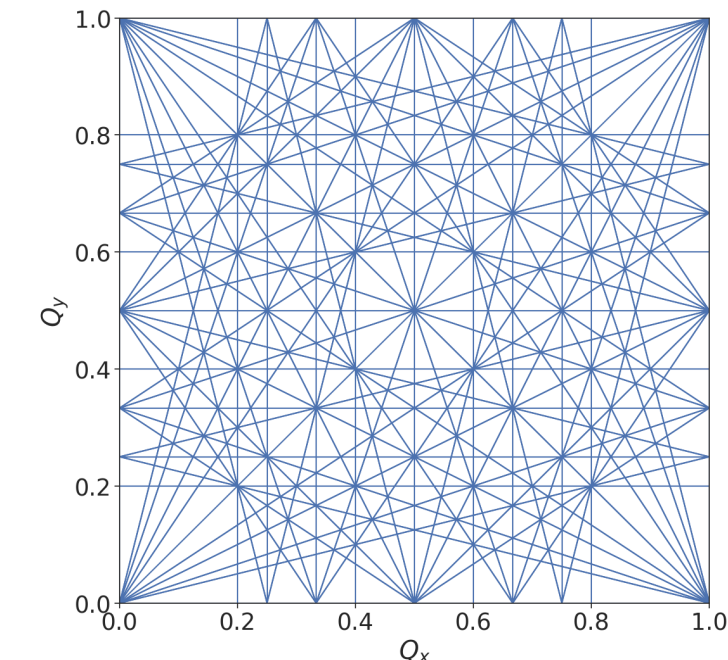


Figure 2.6.: Tune diagram with resonances lines excited by multipoles up to decapole ($n \leq 5$). The working point of the machine is chosen in an area where few lines are present.

2. Concepts of Accelerator Physics

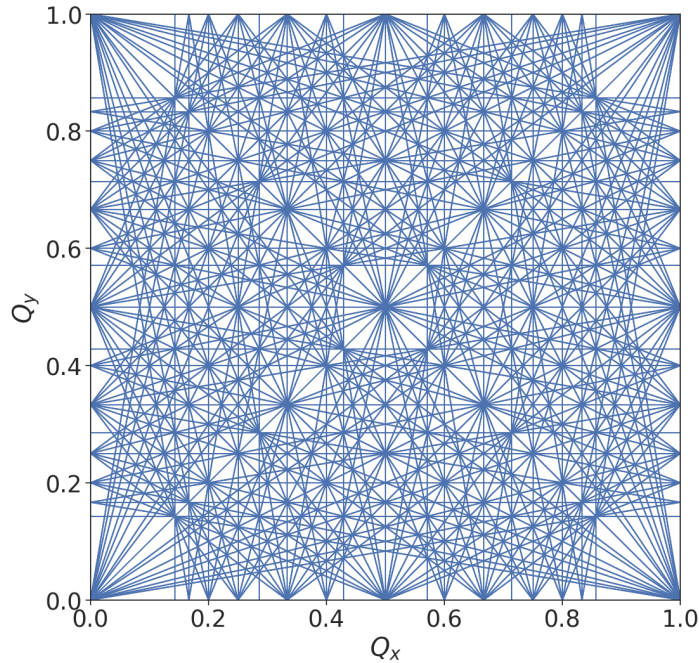


Figure 2.7.: Tune diagram with resonances lines excited by multipoles up to decatetrapole ($n \leq 7$). When considering higher orders, it becomes apparent that the beam will inevitably hit several resonances.

Optics Measurements and Corrections

Contents

3.1.	Beam Instrumentation	30
3.1.1.	Beam Position Monitors	30
3.1.2.	Beam Loss Monitors	31
3.1.3.	AC-Dipole	31
3.2.	Optics Measurements	32
3.2.1.	Turn by Turn	32
3.2.2.	Chromaticity	32
	Procedure	32
	Analysis	33
3.3.	Correction Principles	35
3.3.1.	Response Matrix	35
	Example	36
3.3.2.	Chromaticity	37

3. Optics Measurements and Corrections

3.1. Beam Instrumentation

3.1.1. Beam Position Monitors

Beam Position Monitors (BPMs) are one of the most utilized and essential elements of beam diagnostics in particle accelerators. In the LHC, most of the BPMs are dual plane, and thus composed of four electrodes, distributed as two per plane. The BPM system consists of over than 550 BPMs per beam, distributed along the ring, in the arcs and the IPs. The most common type, the *curved-button*, shown in Fig. 3.1a, is typically placed near quadrupoles [13].



(a) Curved-button "BPM" type BPM of the LHC [13].

(b) Stripline "BPMSW" type BPM of the LHC [13].

Other pickups such as the *stripline*, shown in Fig. 3.1b, albeit more complex and expensive, offer a better signal to noise ratio and are capable of identifying the direction of the beam [13]. Such features are essential for the LHC, were both beams travel through the same aperture at the IPs.

The BPM response is not linear with the beam position, which requires a post-processing not systematically implemented in accelerators beam diagnostics systems. LHC's BPMs have been simulated and polynomials fitted to minimize this response error [14].

3.1.2. Beam Loss Monitors

Beam Loss Monitors are detectors mounted on various elements of the accelerator, such as magnets or collimators, to detect abnormal losses of particles. They play a crucial role in the protection of the machine, triggering a dump when losses exceed the threshold set for their respective element. BLMs use ionization chambers, working on the same principle as simple Geiger counters: a tube filled with gas, in presence of a high voltage.

Dashboards in the control room are regularly used to monitor the losses along the ring when performing optics measurements, as those prove to often be destructive.

3.1.3. AC-Dipole

The AC dipole of the LHC is a crucial component for optics studies. Its primary function is to excite the beam into large coherent oscillation, achieved by applying a sinusoidally oscillating dipole field [15]. By ramping up and down adiabatically the field, large coherent oscillations can be produced without any decoherence or emittance growth. Figure 3.2 shows an example of a measurement made with an AC-Dipole. Exciting the beam to large amplitudes make the study of linear optics, such as beta-beating easier, and that of non linear optics such as resonances possible.

The AC-Dipole is set to oscillate at a frequency Q_d , different from the natural tune of the machine Q and thus introduces systematic effects that needs to be compensated during the optics analysis. The new orbit of a particle under the influence of the AC-Dipole, at turn number n and observation point s , is given by [16]:

$$z(s, n) = \frac{BL}{4\pi\rho\delta_z} \cdot \sqrt{\beta_z(s)\beta_{z,0}} \cdot \cos(2\pi Q_{d,z}n + \phi_z(s) + \phi_{z,0}), \quad (3.1)$$

3. Optics Measurements and Corrections

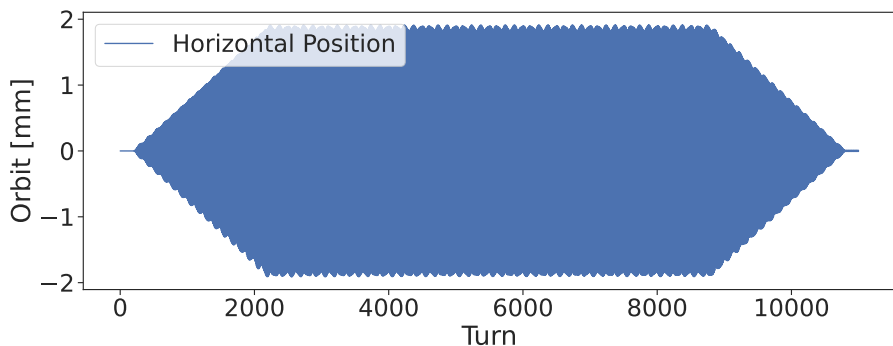


Figure 3.2.: Simulated turn by turn data with an AC-Dipole first ramping up then down.

where B is the amplitude of the oscillating magnetic field, L the length of the AC-Dipole, $B\rho$ the magnetic rigidity, δ the difference between Q_d and Q , β and β_0 the beta function at the observed point and the AC-Dipole, ϕ and ϕ_0 the phase advance at the observed point and of the AC-Dipole.

3.2. Optics Measurements

3.2.1. Turn by Turn

3.2.2. Chromaticity

Procedure

Chromaticity measurements are typically performed by varying the RF frequency to induce a change of momentum offset δ , while measuring the tune. The momentum offset δ being related to the RF frequency and the momentum compaction factor α_c :

3.2. Optics Measurements

$$\delta = -\frac{1}{\alpha_c} \cdot \frac{\Delta f_{RF}}{f_{RF,nominal}} \quad (3.2)$$

Frequency steps of 20Hz every 30 secondes are usually taken to compromise between number of data points, precision of the tune estimate, and duration of the measurement. Once beam losses, registered by the BLMs are deemed too high, the frequency is reverted back to its nominal value in larger steps. The same procedure is then re-applied in the negative. Figure 3.3 shows a typical RF scan performed to measure chromaticity in the LHC.

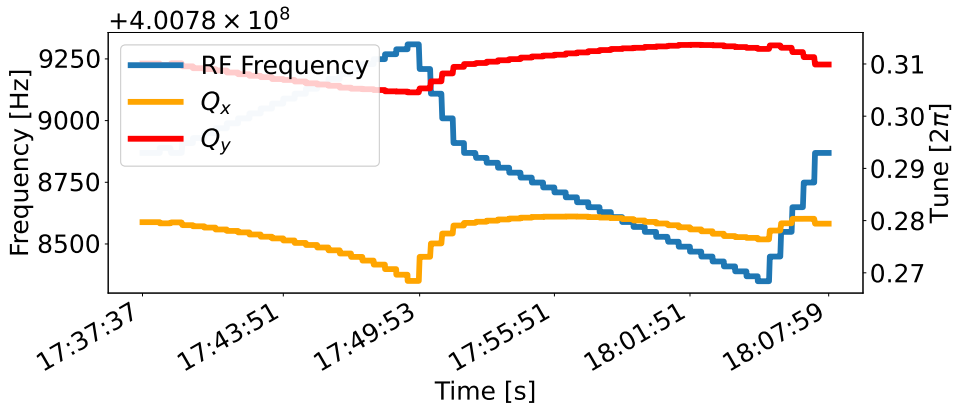


Figure 3.3.: Observation of the tune dependence on momentum offset, created by a shift of RF frequency.

Analysis

Once the tunes have been acquired and the momentum offset computed via Eq. (3.2), the chromaticity function (see Eq.(2.27)) can be used to fit the measured data and retrieve each order.

As part of work for this thesis, a custom tool was developed, in order to

3. Optics Measurements and Corrections

ease such analysis of chromaticity measurements. This tool, the Non-Linear Chromaticity GUI [17], is composed of several parts:

- Data extraction from CERN data servers (Timber, NXCAL)
- Tune cleaning and standard deviation calculation
- Chromaticity fit up to 7th order
- Corrections of chromaticity and resonance driving terms

Fits up to the third and fifth order using this tool can be seen in Fig.3.4.

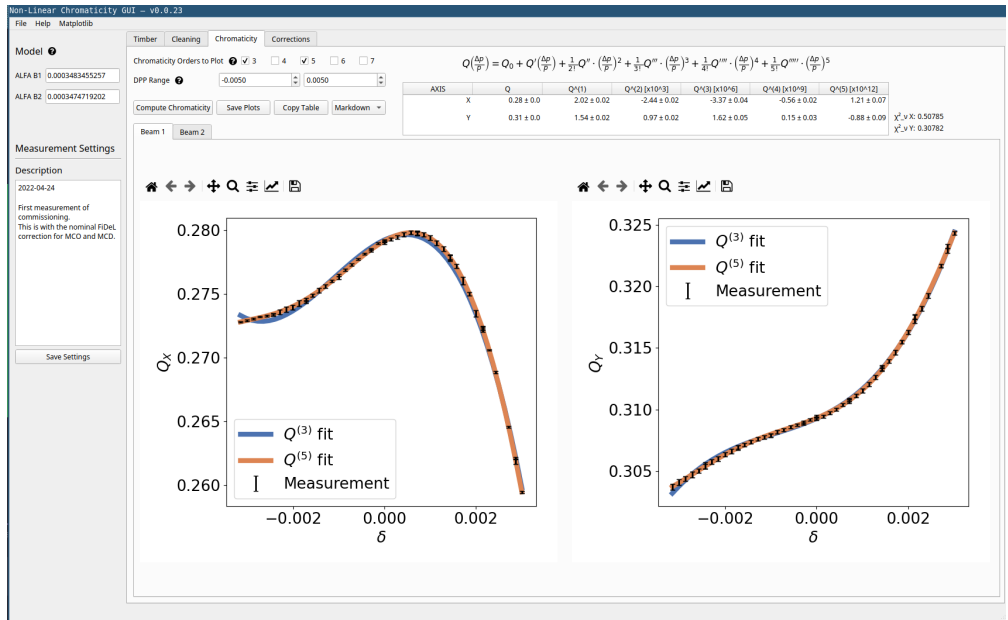


Figure 3.4.: *Non-Linear Chromaticity GUI* program, used to automatize chromaticity analysis.

 3.3. Correction Principles

3.3. Correction Principles

3.3.1. Response Matrix

A response matrix is a linear equation system that describes the change of an observable for a set of individual multipole strengths. By taking the pseudo-inverse of this matrix and multiplying it to the measured observables, a set of corrector strengths if obtained that can replicate the measured value. Taking the opposite sign then gives a correction. This technique is routinely used to correct, amongst others, β -beating as well as Resonance Driving Terms. In situations where measurements are taken at each BPM for a particular observable, the corresponding response matrix ends up containing over 500 values per corrector, for a single beam.

Individual MAD-X simulations are run with a single multipole powered at a time. The resulting parameter values (e.g. β -beating) are then compared to those obtained from a simulation without any powering, allowing to determine the specific impact of each multipole.

A response matrix is thus created following Eq. (3.3), for a matrix of observables O , a reference matrix of observables without any corrector O_R and a fixed multipole strength k . Given measured data M , the set of correctors needed to compensate the values can be obtained by taking the pseudo-inverse of the matrix in Eq. (3.4).

$$R = (O - O_R) \cdot \frac{1}{k} \quad (3.3)$$

$$\begin{bmatrix} k_1 \\ \vdots \\ k_n \end{bmatrix} = -(R^+ \cdot M) \quad (3.4)$$

Response matrices are very versatile and can combine several observables

3. Optics Measurements and Corrections

to be corrected by the same multipoles. One example, detailed later in this thesis, is the third order chromaticity and the resonance driving term f_{1004} , both contributed to by decapoles.

Example

In this example, simulations are run with MAD-X PTC to correct the third chromaticity in the LHC. Q''' is taken from `ptc_normal` for each beam and axis, with MCDs, decapole correctors, powered with a fixed strength one at a time. A scaling factor is applied to get the change of chromaticity for one unit of K_5 . 8 correctors are used, which strengths are denoted k_1 through k_8 . Transposes are only used to make the equations easier to display.

The values in Tab.3.1 are corrected via Eq. (3.6) after having built the response matrix in Eq. (3.5).

Observable	Value
Q'''_x	-666111
Q'''_y	121557

Table 3.1.: Example chromaticity values to correct via a response matrix

$$R = \left(\begin{array}{c} \text{Individual} \\ \text{simulations} \end{array} \right) \left(\begin{array}{cc} Q'''_x & Q'''_y \\ \underbrace{\begin{bmatrix} -155899 & 122004 \\ -254584 & 138368 \\ -122715 & 106709 \\ -218597 & 110686 \\ -134140 & 106463 \\ -245791 & 118951 \\ -147035 & 116544 \\ -219537 & 112317 \end{bmatrix}}^T & \underbrace{\begin{bmatrix} 5135 \\ 8470 \end{bmatrix}}_{\text{Reference}} \\ - \end{array} \right) \cdot \underbrace{\frac{1}{-1000}}_{\text{Corrector strength}}. \quad (3.5)$$

$$\left. \begin{array}{l} k_1 \\ k_2 \\ k_3 \\ k_4 \\ k_5 \\ k_6 \\ k_7 \\ k_8 \end{array} \right\} = -R^+ \cdot \left(\begin{array}{c} -1235 \\ 1032 \\ -1394 \\ 1449 \\ -1043 \\ 1864 \\ -1187 \\ 1369 \end{array} \right) \right\} \text{Measured values} \quad (3.6)$$

3.3.2. Chromaticity

As per the placement of the MCO and MCD spool piece correctors in the LHC layout [18], β -functions at their location are slightly different from arc to arc. This slight imbalance leads theoretically to the possibility of correcting the horizontal and vertical axes of the second and third order chromaticity independently, via a response matrix approach. In practice, the required strength to do so would exceed those of the design of the correctors.

Another way to correct the chromaticity is via a global uniform trim, where every available corrector is powered to the same strength. Simulations are run with `ptc_normal` via MADX-PTC to obtain the response in chromaticity for a given strength. Chromaticity being linear with multipole strength, an affine function can be determined for each axis. Figure 3.5 shows a simulation with several MCD strengths, highlighting this linear relation between Q''' and K_5 , while Equation (3.7) shows an example of such functions computed at injection energy for the 2022 optics.

3. Optics Measurements and Corrections

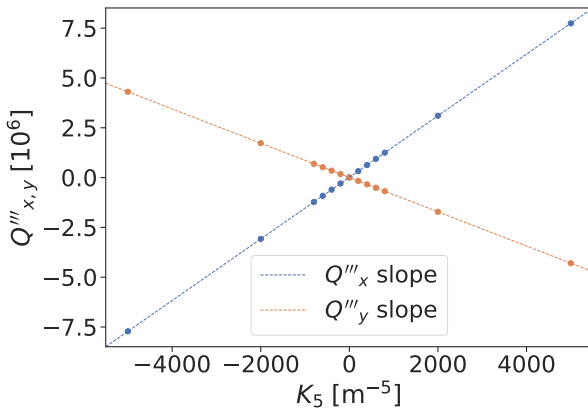


Figure 3.5.: Linear relation between the third order chromaticity and decapole corrector strengths, simulated with MADX-PTC.

$$\begin{aligned} Q'''_x &= 1533 \cdot \Delta K_5 + 6680 \\ Q'''_y &= -860 \cdot \Delta K_5 + 5647 \end{aligned} \quad (3.7)$$

Only the linear part is relevant, as the offset is generated by other multipoles and field errors. It is thus constant for a configuration where only the relevant spool pieces are used.

Corrections involve minimizing both axes, typically where Q'''_x meets Q'''_y :

$$\Delta K_5 = -\frac{(Q'''_x - Q'''_y)}{\text{slope}_{Q'''_x} - \text{slope}_{Q'''_y}} \quad (3.8)$$

4

Decapole Measurements, Corrections and Modelling in the LHC

4

Contents

4.1.	Motivation	40
4.2.	Non-Linear Chromaticity	41
4.3.	Chromatic Amplitude Detuning	41
4.4.	Resonance Driving Terms	41
4.4.1.	Decapolar Contribution	42
4.4.2.	Lower Order Contributions	42
4.5.	Impact of Decapolar Fields	42
4.6.	Integrating Decay	42

4.1. Motivation

The decapole fields in the LHC have been studied since Run 1 via chromaticity measurements [19–21]. The third order of the non-linear chromaticity, Q''' , generated for the most part by decapoles, has shown a consistent discrepancy at injection energy between its expected value in simulation and that observed in beam-based measurements. Figure 4.1 highlights this discrepancy.

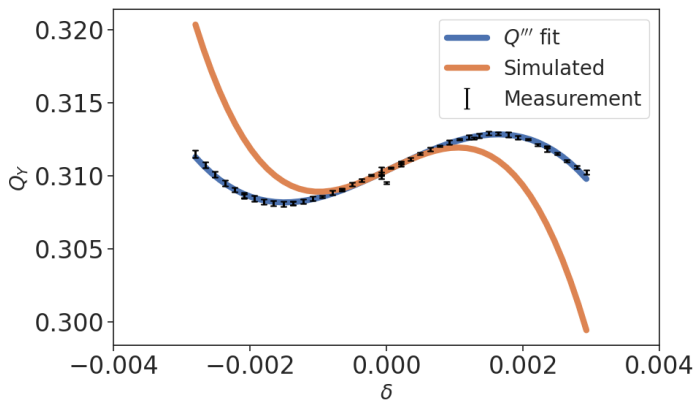


Figure 4.1.: Measured and simulated chromaticity at injection energy without octupolar and decapolar corrections.

This discrepancy poses a significant problem, as the operational corrections are derived from simulations. It is thus observed that Q''' is over-corrected by an almost factor 2, resulting in an effectively un-corrected third order chromaticity. Chromaticity measurements have thus been repeated during LHC’s Run 3 and complemented by beam-based corrections.

While non-linear chromaticity provides an easy measurement of decapolar fields, it does not permit alone to understand where the discrepancy originates from. New measurements were therefore undertaken to better understand the decapolar fields via observables never studied before:

- Bare Chromaticity, chromaticity with octupolar and decapolar correctors turned off.
- Chromatic Amplitude Detuning, tune shift dependant on both the action and the momentum offset.
- Resonance Driving Term f_{1004} , contributing to a resonance close the working point.

4.2. Non-Linear Chromaticity

Measurements were taken during 2022 Commissioning for

- Beam Test
- Commissioning
 - FiDeL
 - Q[”] corr
 - Q[”] corr
- 60° optics

Also during MD6864, 2022-10-19, for the bare machine

Also 2022-11-06, measurement at 30cm, flat top.

High order α_c .

Radial loop instead of formula.

4.3. Chromatic Amplitude Detuning

4.4. Resonance Driving Terms

Measurements

4. Decapole Measurements, Corrections and Modelling in the LHC

- 2022 Q” and Q”’ corrs 2022-04-24
- 2022-10-19 Virgin machine
- 2023-easter (FiDeL)
- 2023-06-14 MD9549 (FiDeL and Q”’/ RDT corr)

Bring up effect of KCO on RDT f1004

4.4.1. Decapolar Contribution

4.4.2. Lower Order Contributions

4.5. Impact of Decapolar Fields

4.6. Integrating Decay

5

Very High Order Field Measurement in the LHC

Contents

5.1.	First Measurement of Fourth and Fifth Order Chromaticity	44
5.2.	INTRODUCTION	44
5.3.	NL-CHROMATICITY MEASUREMENTS	45
5.3.1.	Nominal Corrections	45
5.3.2.	Beam-Based Corrections	47
5.3.3.	$Q^{(4)}$ and $Q^{(5)}$ fit quality	48
5.4.	NL-CHROMATICITY MODEL	50
5.5.	CONCLUSIONS AND OUTLOOK	51
5.6.	First Measurement of Dodecapole RDTs	52

5.1. First Measurement of Fourth and Fifth Order Chromaticity

1. IPAC paper basically

5.2. INTRODUCTION

Non-Linear chromaticity measurements at injection have been performed since Run 1 [[maclean:ipac11-wepc078](#), [maclean:ipac16-thpmr039](#), [20](#), [22](#)]. Those measurements, made by varying the RF frequency while observing the resulting tune change, have been carried out with a momentum offset of up to $\delta = \pm 2.2 \times 10^{-3}$, which led to the observation of the third order term of the non-linear chromaticity.

5

During the commissioning of Run 3, a new collimator sequence was introduced, allowing wider momentum offset measurements, within $\delta \in [-3.2 \times 10^{-3}, 3.7 \times 10^{-3}]$. This improved setup led to the observation of the fourth and fifth order terms at injection energy, denoted $Q^{(4)}$ and $Q^{(5)}$ respectively, produced to first order by dodecapoles and tetradecapoles (see section NL-CHROMATICITY MODEL):

$$\begin{aligned} Q(\delta) = Q_0 + Q'\delta + \frac{1}{2!}Q''\delta^2 + \frac{1}{3!}Q'''\delta^3 \\ + \frac{1}{4!}Q^{(4)}\delta^4 + \frac{1}{5!}Q^{(5)}\delta^5 + \mathcal{O}(\delta^6). \end{aligned} \quad (5.1)$$

The momentum offset δ is related to the RF frequency and the momentum compaction factor:

$$\delta = -\frac{1}{\alpha_c} \frac{\Delta f_{RF}}{f_{RF,nominal}}.$$

The model α_c used is 3.48×10^{-4} for beam 1 and 3.47×10^{-4} for beam 2. Via this relation, a change of 140Hz of the RF frequency corresponds to a momentum offset of about -0.001 .

Results of $Q^{(4)}$ and $Q^{(5)}$ measurements are presented, along with a comparison to the model.

5.3. NL-CHROMATICITY MEASUREMENTS

Two chromaticity measurements were performed with different settings. The first one used the nominal correction strengths for octupole and decapole corrector magnets, derived from magnetic measurements, where the second one used beam-based corrections for the same elements, computed from measurements. Those two measurements have a respective momentum-offset range of $[-3.1 \times 10^{-3}, 3.1 \times 10^{-3}]$ and $[-3.2 \times 10^{-3}, 3.7 \times 10^{-3}]$.

5.3.1. Nominal Corrections

A first chromaticity measurement was performed during the LHC beam commissioning in April 2022. The horizontal and vertical tunes were set to 0.28 and 0.31. Q' was reduced to a value of 2 to allow for a better identification of the higher order terms. The standard measurement procedure was then applied, by varying the RF frequency to induce a change in momentum offset. Frequency steps of 20Hz were taken roughly every 30 seconds, to allow for a precise tune measurement. Once beam losses, registered by the beam loss monitors (BLM), are deemed too high the frequency is reverted back to its nominal frequency in larger steps. Figure 5.1 shows a typical RF scan performed to measure chromaticity.

At very high momentum-offsets, the Base-Band Tune system (BBQ) [23, 24] was found not to give reliable tune measurements. A new approach using custom post-processing of the raw BBQ turn-by-turn data was therefore developed, giving more precise tune measurements by performing spectral analysis with an increased number of turns to improve the signal to noise ratio. Further cleaning is then applied by removing outliers and identified noise lines.

5. Very High Order Field Measurement in the LHC

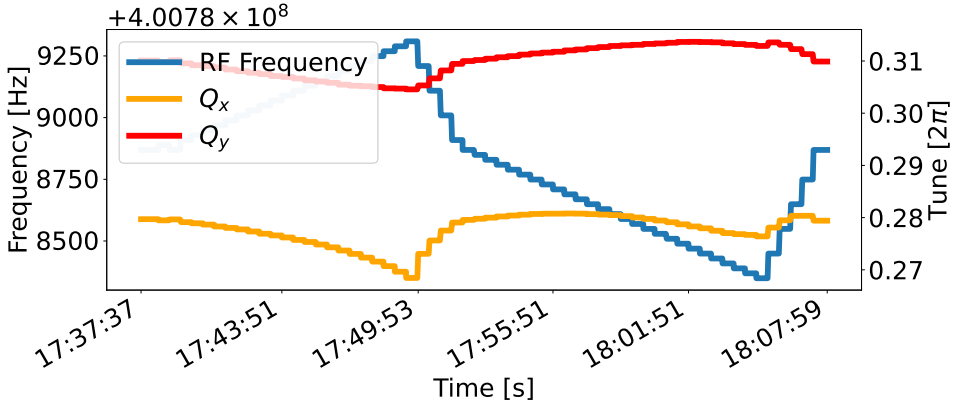


Figure 5.1.: Observation of the tune dependence on momentum offset, created by a shift of RF frequency.

5

The octupole and decapole correctors were set to their nominal settings. Results of this initial measurement are shown in Tab. 5.1. Lower order chromaticities such as Q' and Q'' are consistent with previous measurements [20].

	$Q^{(2)}[10^3]$	$Q^{(3)}[10^6]$	$Q^{(4)}[10^9]$	$Q^{(5)}[10^{12}]$
B1				
X	-2.44 ± 0.02	-3.36 ± 0.04	-0.56 ± 0.02	1.20 ± 0.07
Y	0.97 ± 0.02	1.62 ± 0.05	0.15 ± 0.03	-0.88 ± 0.09
B2				
X	-2.45 ± 0.03	-2.72 ± 0.08	-1.00 ± 0.05	0.15 ± 0.14
Y	0.79 ± 0.03	1.54 ± 0.06	0.24 ± 0.04	-0.74 ± 0.13

Table 5.1.: Terms of the high order chromaticity obtained during Run 3 commissioning in April 2022, with nominal corrections.

Due to the momentum offset being zero several times during the measurement, it was possible to determine that the tune drift is negligible. The measurement was also performed after an extended period at injection energy, where the b_3 decay is small and not causing any change in the first order chromaticity.

The fitted curve for the chromaticity function is shown in Fig. 5.2. It can be seen that a higher order polynomial is beneficial for the fit, as discussed further in "Q⁽⁴⁾ and Q⁽⁵⁾ fit quality".

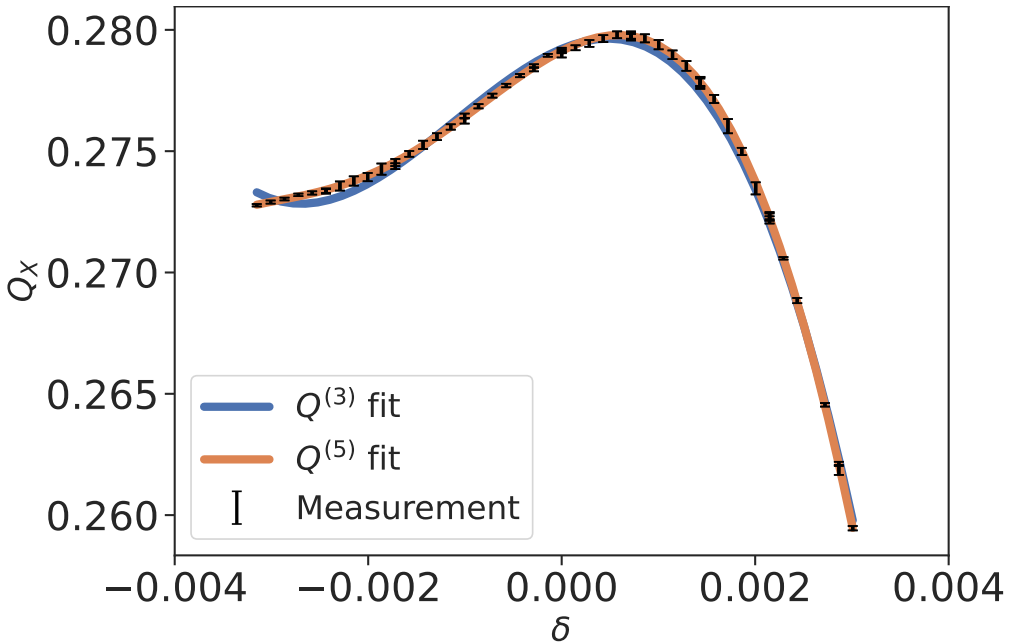


Figure 5.2.: Beam 1 measurement of higher order chromaticity terms with nominal corrections used during operation. Fits are up to the third and fifth order.

5.3.2. Beam-Based Corrections

After correcting the second and third order chromaticities via the octupole and decapole correctors, a second measurement was performed. A uniform trim on all the correctors of each class was applied for each beam, resulting in a global correction. A total of four circuits were unavailable for the octupoles, three for beam 1 and one for beam 2, resulting in larger corrections for beam 1.

5. Very High Order Field Measurement in the LHC

Corrections applied on top of the nominal settings [20] for the octupoles and decapoles are shown in Tab. 5.2.

Beam	$K_4[\text{m}^{-4}]$	$K_5[\text{m}^{-5}]$
1	+3.2973	+1610
2	+2.1716	+1618

Table 5.2.: Corrections applied on top of the nominal octupole and decapole correctors strengths.

Figure 5.3 shows the chromaticity fit after the beam-based minimization of Q'' and Q''' , while Tab. 5.3 shows the measured chromaticity.

Previous studies of chromaticity in the LHC only considered fits up to third-order. Including fits up to a fifth order increases the Q''' estimate of both measurements, while improving the fit quality. Q''' for beam 1 with only a fit to the third order would have a value of -0.38×10^6 instead of the -1.02×10^6 obtained with a fifth order fit. Accurately measuring the third order chromaticity is essential in order to correct it.

	$Q^{(2)}[10^3]$	$Q^{(3)}[10^6]$	$Q^{(4)}[10^9]$	$Q^{(5)}[10^{12}]$
B1				
X	-0.62 ± 0.01	-1.02 ± 0.03	-0.63 ± 0.02	1.22 ± 0.05
Y	-0.24 ± 0.01	0.12 ± 0.02	0.04 ± 0.02	-0.56 ± 0.04
B2				
X	-0.85 ± 0.01	-0.64 ± 0.03	-0.58 ± 0.02	1.07 ± 0.06
Y	-0.30 ± 0.02	0.14 ± 0.03	0.16 ± 0.02	-0.66 ± 0.05

Table 5.3.: Terms of higher order chromaticity obtained during Run 3 commissioning in April 2022, with beam-based corrections for Q'' and Q''' .

5.3.3. $Q^{(4)}$ and $Q^{(5)}$ fit quality

The values measured for $Q^{(4)}$ and $Q^{(5)}$ are similar across the two measurements, with nominal and beam-based corrections performed with very different lower

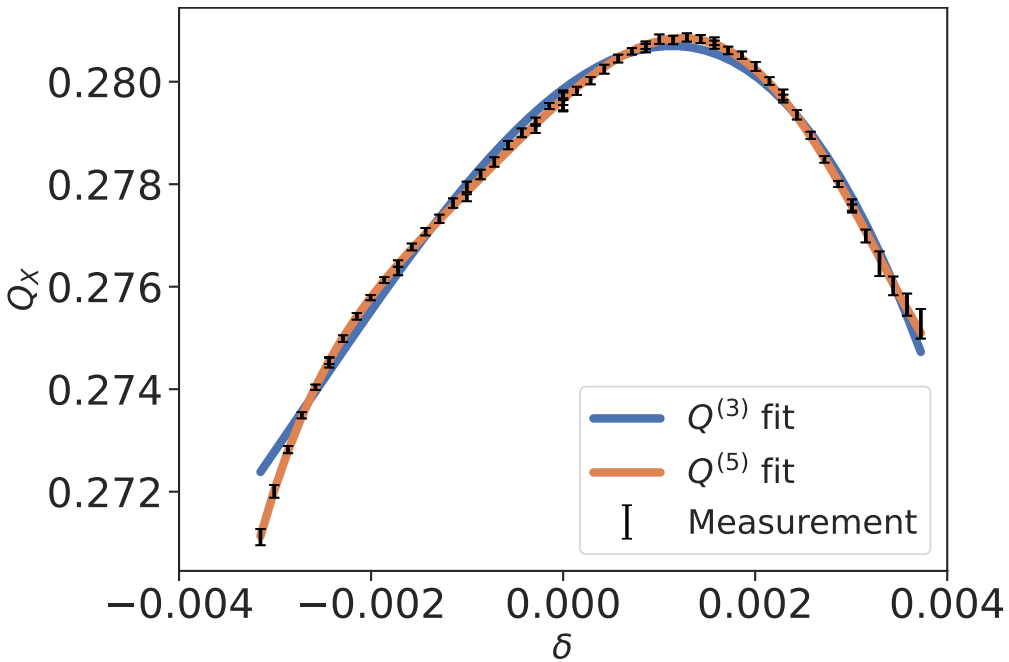


Figure 5.3.: Beam 1 measurement of high order chromaticity terms after application of Q'' and Q''' beam-based corrections on octupole and decapole correctors.

order chromaticity and several hours apart. This reproducibility gives confidence that the measured values are robust. It is to be noted that one exception exists, for the horizontal plane of beam 2, where the measurement with nominal correction settings showed a high correlation between the fourth and fifth order terms, making the fit less reliable.

The reduced chi-square for the last measurement for each fit order is detailed in Tab. 5.4, where it can be seen that a fit above fifth order does not improve the fit quality.

5. Very High Order Field Measurement in the LHC

Plane	$\chi^2_\nu Q^{(3)}$	$\chi^2_\nu Q^{(4)}$	$\chi^2_\nu Q^{(5)}$	$\chi^2_\nu Q^{(6)}$
Beam 1				
X	17.9	12.1	1.8	1.47
Y	3.0	2.2	0.7	0.7
Beam 2				
X	17.3	7.1	1.8	1.76
Y	2.9	2.8	1.0	1.0

Table 5.4.: Reduced χ^2_ν values for each order of fit, taken from the last commissioning measurement.

5.4. NL-CHROMATICITY MODEL

The model of the LHC is based on MADX and WISE field errors [25]. To compute the chromaticity, simulations are run via the Polymorphic Tracking Code (PTC), with field errors from sextupole to hexadecapole loaded and applied on all magnets. Simulation results are shown in Tab. 5.5.

Table 5.6 shows the ratio between measured and simulated high-order chromaticity. The measured $Q^{(5)}$ shows a consistent discrepancy with the model, larger by about a factor 2.

Plane	$Q^{(4)}[10^9]$	$Q^{(5)}[10^{12}]$
Beam 1		
X	-0.2 ± 0.1	0.7 ± 0.1
Y	0.1 ± 0.1	-0.3 ± 0.1
Beam 2		
X	-0.2 ± 0.1	0.8 ± 0.1
Y	0.1 ± 0.1	-0.4 ± 0.1

Table 5.5.: Simulated high order chromaticity terms via PTC, including field errors from b_3 to b_8 with the previous beam-based corrections.

Simulations with only b_6 and b_7 field errors have been run to assess the contribution of lower order magnets to the fifth order chromaticities. The results

5.5. CONCLUSIONS AND OUTLOOK

Plane Measurement	$Q^{(5)}$ ratio	
	first	second
Beam 1		
X	1.8 ± 0.1	1.8 ± 0.1
Y	2.7 ± 0.3	1.7 ± 0.1
Beam 2		
X		1.6 ± 0.1
Y	2.2 ± 0.4	1.9 ± 0.2

Table 5.6.: Ratios of the measured to simulated fifth order chromaticity term for both first and second measurements. The values are taken from tables 5.1, 5.3 and 5.5. The fit with high correlation was not included.

strongly imply that the tetradecapole errors are the main contributors to $Q^{(5)}$, as can be seen in Fig. 5.4. Fringe fields and skew multipoles have been found to have a negligible impact. Ongoing studies are assessing the contribution of β -beating, linear coupling and alignment errors to those estimates.

5.5. CONCLUSIONS AND OUTLOOK

A wider momentum offset range, combined with new analysis techniques permitted the observation of fourth and fifth order chromaticity for the first time in the LHC. Reproducible values were measured with different machine configurations. Preliminary simulations show that the observed values do not match well with the LHC non-linear model. A factor 2 is observed between beams and planes for $Q^{(5)}$, which may point to a systematic error in the b7 error model.

Correction of the measured higher order chromaticity terms is not possible, due to the lack of adequate correctors in the LHC. It is nevertheless interesting to characterize the higher order errors for an effective model and understand the effect a higher order fit has on lower order terms. Precise measurement of those lower chromaticity terms is required in order to effectively correct them.

5. Very High Order Field Measurement in the LHC

Higher order terms have thus to be taken into account.

The current range of momentum offset is deemed sufficient to measure higher order chromaticity. Attempts will, however, be taken to increase that range and assess if such a wider range can refine the estimate of $Q^{(4)}$ and $Q^{(5)}$.

5.6. First Measurement of Dodecapole RDTs

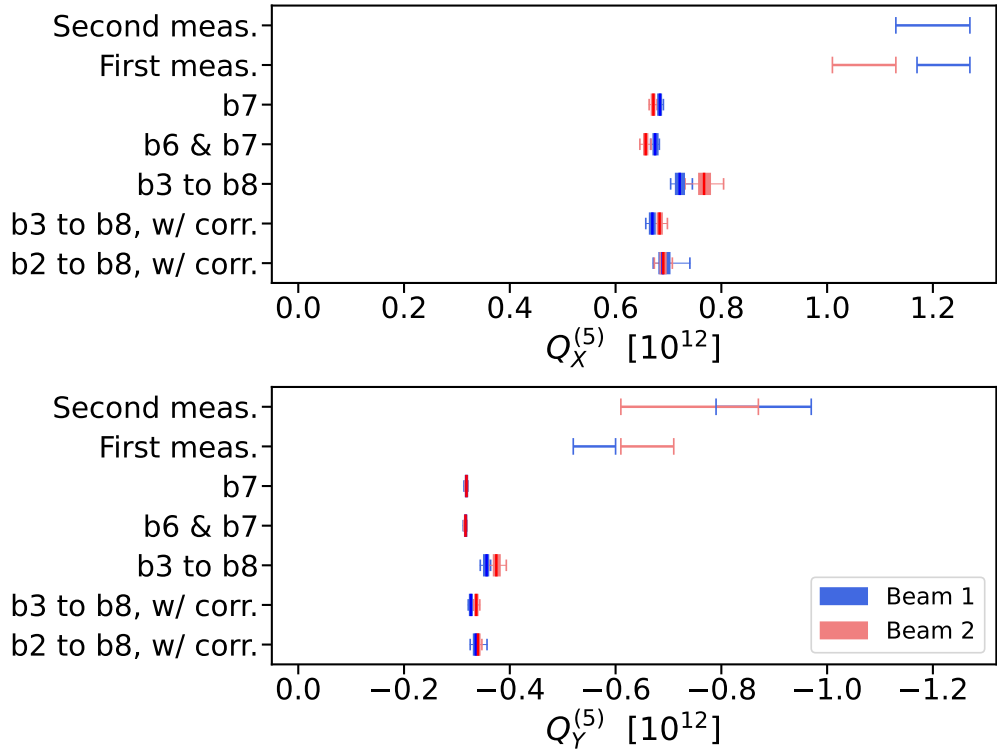


Figure 5.4.: Measured and simulated fifth order chromaticity. The simulations are done via PTC and include different multipole errors, some of them further include the nominal corrections for b_3 , b_4 and b_5 . The b_2 errors, applied on dipoles and quadrupoles, generate beta-beating. The measurement with a high correlation is not included.

6

Skew Octupole Fields in the LHC

Contents

6.1.	Correction of skew octupole Fields at Top Energy	56
6.2.	Correction of Skew Octupole Fields at Injection Energy	56
6.3.	Skew Octupolar Fields from Landau Octupoles	57

6

6.1. Correction of skew octupole Fields at Top Energy

1. RDT Measurements
2. Orthogonality of correctors
3. Response Matrix
4. Correction
5. Comparison to 2018

6.2. Correction of Skew Octupole Fields at Injection Energy

6

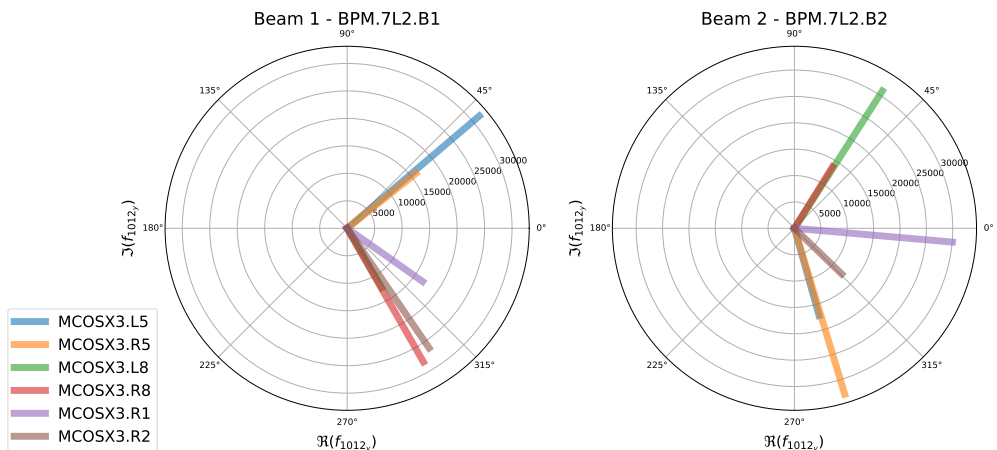


Figure 6.1.

6.3. Skew Octupolar Fields from Landau Octupoles

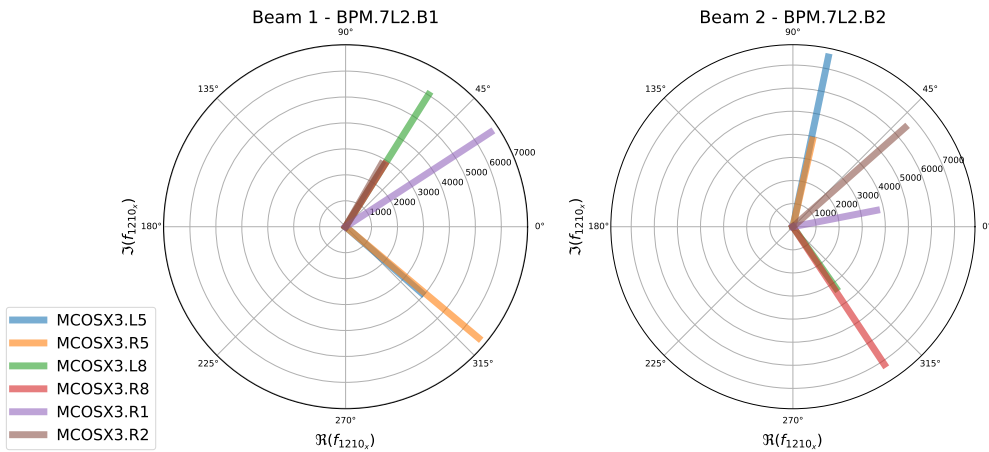
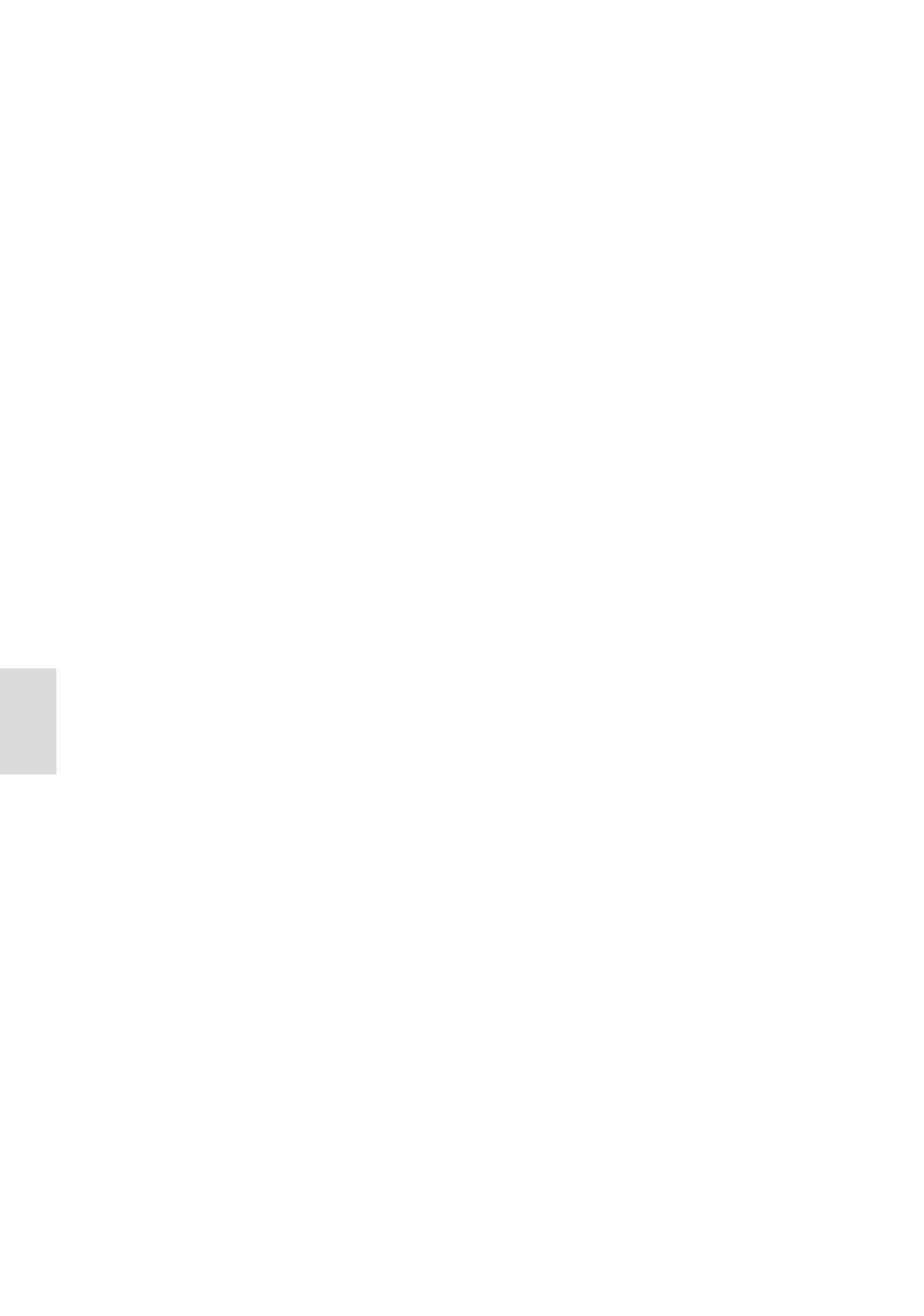


Figure 6.2.

6.3. Skew Octupolar Fields from Landau Octupoles



A

Units and Conversions

A.1. Physical Constants

Name	Symbol	Value	Unit
Speed of light in vacuum	c	2.99792458×10^8	m/s
Elementary charge	e	$1.60217663 \times 10^{-9}$	C

Table A.1.: Physical Constants

A.2. Units

A.3. Conversions

A

A

B

Resonance Driving Terms

This appendix intends to clarify where Resonance Driving Terms can be seen in the frequency spectrum, what resonance they contribute to and what their action dependance is. The number of valid RDTs indeed grows rapidly with the magnet order n , and is given by the following combinations:

$$C(n+3, 3) - C(n+1, 1) - [(n+1)\%2] \cdot C\left(\frac{n}{2} + 1, 1\right). \quad (\text{B.1})$$

Several different RDTs can contribute to the same line, which can be observed in the horizontal or vertical spectrum. The tables below describe which RDTs contribute to a specific combination of line and plane. All tables have been computed up to the order 6, for decapoles. The line columns represents (Q_x, Q_y) . For example $(-1, 2)$ is $-1Q_x + 2Qy$.

As a reminder, for a given RDT f_{jklm} , we will observe:

B

B. Resonance Driving Terms

$$\begin{aligned}
 (j - k)Q_x + (l - m)Q_y = p \in \mathbb{N} & \quad \text{excited resonance} \\
 H(1 - j + k, m - l) & \quad \text{horizontal line, if } j \neq 0 \\
 V(k - j, 1 - l + m) & \quad \text{vertical line, if } l \neq 0.
 \end{aligned} \tag{B.2}$$

The amplitude of each line is given by:

$$\begin{aligned}
 |H_{f_{jklm}}| &= 2j(2I_x)^{\frac{j+k-1}{2}}(2I_y)^{\frac{l+m}{2}}|f_{jklm}| \\
 |V_{f_{jklm}}| &= 2l(2I_x)^{\frac{j+k}{2}}(2I_y)^{\frac{l+m-1}{2}}|f_{jklm}|.
 \end{aligned} \tag{B.3}$$

According to equations B.2 and B.3, it can be seen that many RDTs will no generate any line and thus can not be observed.

B.1. Frequency Spectrum Lines

B.1.1. Horizontal Axis

H-line	RDTs
(-5, 0)	f6000
(-4, -1)	f5010
(-4, 0)	f5000
(-4, 1)	f5001
(-3, -2)	f4020
(-3, -1)	f4010
(-3, 0)	f4000, f4011, f5100
(-3, 1)	f4001
(-3, 2)	f4002
(-2, -3)	f3030
(-2, -2)	f3020

H-line	RDTs
(-2, -1)	f3010, f3021, f4110
(-2, 0)	f3000, f3011, f4100
(-2, 1)	f3001, f3012, f4101
(-2, 2)	f3002
(-2, 3)	f3003
(-1, -4)	f2040
(-1, -3)	f2030
(-1, -2)	f2020, f2031, f3120
(-1, -1)	f2010, f2021, f3110
(-1, 0)	f2000, f2011, f3100, f2022, f3111, f4200
(-1, 1)	f2001, f2012, f3101
(-1, 2)	f2002, f2013, f3102
(-1, 3)	f2003
(-1, 4)	f2004
(0, -5)	f1050
(0, -4)	f1040
(0, -3)	f1030, f1041, f2130
(0, -2)	f1020, f1031, f2120
(0, -1)	f1010, f1021, f2110, f1032, f2121, f3210
(0, 0)	f1011, f2100, f1022, f2111, f3200
(0, 1)	f1001, f1012, f2101, f1023, f2112, f3201
(0, 2)	f1002, f1013, f2102
(0, 3)	f1003, f1014, f2103
(0, 4)	f1004
(0, 5)	f1005
(1, -4)	f1140
(1, -3)	f1130
(1, -2)	f1120, f1131, f2220
(1, -1)	f1110, f1121, f2210
(1, 1)	f1101, f1112, f2201

B. Resonance Driving Terms

H-line	RDTs
(1, 2)	f1102, f1113, f2202
(1, 3)	f1103
(1, 4)	f1104
(2, -3)	f1230
(2, -2)	f1220
(2, -1)	f1210, f1221, f2310
(2, 0)	f1200, f1211, f2300
(2, 1)	f1201, f1212, f2301
(2, 2)	f1202
(2, 3)	f1203
(3, -2)	f1320
(3, -1)	f1310
(3, 0)	f1300, f1311, f2400
(3, 1)	f1301
(3, 2)	f1302
(4, -1)	f1410
(4, 0)	f1400
(4, 1)	f1401
(5, 0)	f1500

B.1.2. Vertical Axis

V-line	RDTs
(-5, 0)	f5010
(-4, -1)	f4020
(-4, 0)	f4010
(-4, 1)	f4011
(-3, -2)	f3030

V-line	RDTs
(-3, -1)	f3020
(-3, 0)	f3010, f3021, f4110
(-3, 1)	f3011
(-3, 2)	f3012
(-2, -3)	f2040
(-2, -2)	f2030
(-2, -1)	f2020, f2031, f3120
(-2, 0)	f2010, f2021, f3110
(-2, 1)	f2011, f2022, f3111
(-2, 2)	f2012
(-2, 3)	f2013
(-1, -4)	f1050
(-1, -3)	f1040
(-1, -2)	f1030, f1041, f2130
(-1, -1)	f1020, f1031, f2120
(-1, 0)	f1010, f1021, f2110, f1032, f2121, f3210
(-1, 1)	f1011, f1022, f2111
(-1, 2)	f1012, f1023, f2112
(-1, 3)	f1013
(-1, 4)	f1014
(0, -5)	f0060
(0, -4)	f0050
(0, -3)	f0040, f0051, f1140
(0, -2)	f0030, f0041, f1130
(0, -1)	f0020, f0031, f1120, f0042, f1131, f2220
(0, 0)	f0021, f1110, f0032, f1121, f2210
(0, 2)	f0012, f0023, f1112
(0, 3)	f0013, f0024, f1113
(0, 4)	f0014
(0, 5)	f0015

B. Resonance Driving Terms

V-line	RDTs
(1, -4)	f0150
(1, -3)	f0140
(1, -2)	f0130, f0141, f1230
(1, -1)	f0120, f0131, f1220
(1, 0)	f0110, f0121, f1210, f0132, f1221, f2310
(1, 1)	f0111, f0122, f1211
(1, 2)	f0112, f0123, f1212
(1, 3)	f0113
(1, 4)	f0114
(2, -3)	f0240
(2, -2)	f0230
(2, -1)	f0220, f0231, f1320
(2, 0)	f0210, f0221, f1310
(2, 1)	f0211, f0222, f1311
(2, 2)	f0212
(2, 3)	f0213
(3, -2)	f0330
(3, -1)	f0320
(3, 0)	f0310, f0321, f1410
(3, 1)	f0311
(3, 2)	f0312
(4, -1)	f0420
(4, 0)	f0410
(4, 1)	f0411
(5, 0)	f0510

B.2. Amplitude, Resonances and Lines

This part focuses on individual Resonance Drivings Terms, expliciting what magnet they originte from, what resonance they excite, how they can be observed and what kicks are needed in order to measure them. The amplitude columns implicitely omits the term $|f_{jklm}|$, which depends on K and J .

Amplitude legend:

- I_x : depends only on horizontal amplitude
- I_y : depends only on vertical amplitude
- $I_x I_y$: depends on both horizontal and vertical amplitude

n	jklm	type	resonance	H-line	V-line	Amplitude H	Amplitude V
2	0020	normal	(0, 2)		(0, -1)		$4(2I_y)^{1/2}$
2	2000	normal	(2, 0)	(-1, 0)		$4(2I_x)^{1/2}$	
2	0110	skew	(-1, 1)		(1, 0)		$2(2I_x)^{1/2}$
2	1001	skew	(1, -1)	(0, 1)		$2(2I_y)^{1/2}$	
2	1010	skew	(1, 1)	(0, -1)	(-1, 0)	$2(2I_y)^{1/2}$	$2(2I_x)^{1/2}$
3	0111	normal	(-1, 0)		(1, 1)		$2(2I_x)^{1/2}(2I_y)^{1/2}$
3	0120	normal	(-1, 2)		(1, -1)		$4(2I_x)^{1/2}(2I_y)^{1/2}$
3	1002	normal	(1, -2)	(0, 2)		$2(2I_y)$	
3	1011	normal	(1, 0)	(0, 0)	(-1, 1)	$2(2I_y)$	$2(2I_x)^{1/2}(2I_y)^{1/2}$
3	1020	normal	(1, 2)	(0, -2)	(-1, -1)	$2(2I_y)$	$4(2I_x)^{1/2}(2I_y)^{1/2}$
3	1200	normal	(-1, 0)	(2, 0)		$2(2I_x)$	
3	2100	normal	(1, 0)	(0, 0)		$4(2I_x)$	
3	3000	normal	(3, 0)	(-2, 0)		$6(2I_x)$	
3	0012	skew	(0, -1)		(0, 2)		$2(2I_y)$
3	0021	skew	(0, 1)		(0, 0)		$4(2I_y)$
3	0030	skew	(0, 3)		(0, -2)		$6(2I_y)$
3	0210	skew	(-2, 1)		(2, 0)		$2(2I_x)$
3	1101	skew	(0, -1)	(1, 1)		$2(2I_x)^{1/2}(2I_y)^{1/2}$	

B

B. Resonance Driving Terms

n	jklm	type	resonance	H-line	V-line	Amplitude H	Amplitude V
3	1110	skew	(0, 1)	(1, -1)	(0, 0)	$2(2I_x)^{1/2}(2I_y)^{1/2}$	$2(2I_x)$
3	2001	skew	(2, -1)	(-1, 1)		$4(2I_x)^{1/2}(2I_y)^{1/2}$	
3	2010	skew	(2, 1)	(-1, -1)	(-2, 0)	$4(2I_x)^{1/2}(2I_y)^{1/2}$	$2(2I_x)$
4	0013	normal	(0, -2)		(0, 3)		$2(2I_y)^{3/2}$
4	0031	normal	(0, 2)		(0, -1)		$6(2I_y)^{3/2}$
4	0040	normal	(0, 4)		(0, -3)		$8(2I_y)^{3/2}$
4	0211	normal	(-2, 0)		(2, 1)		$2(2I_x)(2I_y)^{1/2}$
4	0220	normal	(-2, 2)		(2, -1)		$4(2I_x)(2I_y)^{1/2}$
4	1102	normal	(0, -2)	(1, 2)		$2(2I_x)^{1/2}(2I_y)$	
4	1120	normal	(0, 2)	(1, -2)	(0, -1)	$2(2I_x)^{1/2}(2I_y)$	$4(2I_x)(2I_y)^{1/2}$
4	1300	normal	(-2, 0)	(3, 0)		$2(2I_x)^{3/2}$	
4	2002	normal	(2, -2)	(-1, 2)		$4(2I_x)^{1/2}(2I_y)$	
4	2011	normal	(2, 0)	(-1, 0)	(-2, 1)	$4(2I_x)^{1/2}(2I_y)$	$2(2I_x)(2I_y)^{1/2}$
4	2020	normal	(2, 2)	(-1, -2)	(-2, -1)	$4(2I_x)^{1/2}(2I_y)$	$4(2I_x)(2I_y)^{1/2}$
4	3100	normal	(2, 0)	(-1, 0)		$6(2I_x)^{3/2}$	
4	4000	normal	(4, 0)	(-3, 0)		$8(2I_x)^{3/2}$	
4	0112	skew	(-1, -1)		(1, 2)		$2(2I_x)^{1/2}(2I_y)$
4	0121	skew	(-1, 1)		(1, 0)		$4(2I_x)^{1/2}(2I_y)$
4	0130	skew	(-1, 3)		(1, -2)		$6(2I_x)^{1/2}(2I_y)$
4	0310	skew	(-3, 1)		(3, 0)		$2(2I_x)^{3/2}$
4	1003	skew	(1, -3)	(0, 3)		$2(2I_y)^{3/2}$	
4	1012	skew	(1, -1)	(0, 1)	(-1, 2)	$2(2I_y)^{3/2}$	$2(2I_x)^{1/2}(2I_y)$
4	1021	skew	(1, 1)	(0, -1)	(-1, 0)	$2(2I_y)^{3/2}$	$4(2I_x)^{1/2}(2I_y)$
4	1030	skew	(1, 3)	(0, -3)	(-1, -2)	$2(2I_y)^{3/2}$	$6(2I_x)^{1/2}(2I_y)$
4	1201	skew	(-1, -1)	(2, 1)		$2(2I_x)(2I_y)^{1/2}$	
4	1210	skew	(-1, 1)	(2, -1)	(1, 0)	$2(2I_x)(2I_y)^{1/2}$	$2(2I_x)^{3/2}$
4	2101	skew	(1, -1)	(0, 1)		$4(2I_x)(2I_y)^{1/2}$	
4	2110	skew	(1, 1)	(0, -1)	(-1, 0)	$4(2I_x)(2I_y)^{1/2}$	$2(2I_x)^{3/2}$
4	3001	skew	(3, -1)	(-2, 1)		$6(2I_x)(2I_y)^{1/2}$	

B

B.2. Amplitude, Resonances and Lines

n	jklm	type	resonance	H-line	V-line	Amplitude H	Amplitude V
4	3010	skew	(3, 1)	(-2, -1)	(-3, 0)	$6(2I_x)(2I_y)^{1/2}$	$2(2I_x)^{3/2}$
5	0113	normal	(-1, -2)		(1, 3)		$2(2I_x)^{1/2}(2I_y)^{3/2}$
5	0122	normal	(-1, 0)		(1, 1)		$4(2I_x)^{1/2}(2I_y)^{3/2}$
5	0131	normal	(-1, 2)		(1, -1)		$6(2I_x)^{1/2}(2I_y)^{3/2}$
5	0140	normal	(-1, 4)		(1, -3)		$8(2I_x)^{1/2}(2I_y)^{3/2}$
5	0311	normal	(-3, 0)		(3, 1)		$2(2I_x)^{3/2}(2I_y)^{1/2}$
5	0320	normal	(-3, 2)		(3, -1)		$4(2I_x)^{3/2}(2I_y)^{1/2}$
5	1004	normal	(1, -4)	(0, 4)		$2(2I_y)^2$	
5	1013	normal	(1, -2)	(0, 2)	(-1, 3)	$2(2I_y)^2$	$2(2I_x)^{1/2}(2I_y)^{3/2}$
5	1022	normal	(1, 0)	(0, 0)	(-1, 1)	$2(2I_y)^2$	$4(2I_x)^{1/2}(2I_y)^{3/2}$
5	1031	normal	(1, 2)	(0, -2)	(-1, -1)	$2(2I_y)^2$	$6(2I_x)^{1/2}(2I_y)^{3/2}$
5	1040	normal	(1, 4)	(0, -4)	(-1, -3)	$2(2I_y)^2$	$8(2I_x)^{1/2}(2I_y)^{3/2}$
5	1202	normal	(-1, -2)	(2, 2)		$2(2I_x)(2I_y)$	
5	1211	normal	(-1, 0)	(2, 0)	(1, 1)	$2(2I_x)(2I_y)$	$2(2I_x)^{3/2}(2I_y)^{1/2}$
5	1220	normal	(-1, 2)	(2, -2)	(1, -1)	$2(2I_x)(2I_y)$	$4(2I_x)^{3/2}(2I_y)^{1/2}$
5	1400	normal	(-3, 0)	(4, 0)		$2(2I_x)^2$	
5	2102	normal	(1, -2)	(0, 2)		$4(2I_x)(2I_y)$	
5	2111	normal	(1, 0)	(0, 0)	(-1, 1)	$4(2I_x)(2I_y)$	$2(2I_x)^{3/2}(2I_y)^{1/2}$
5	2120	normal	(1, 2)	(0, -2)	(-1, -1)	$4(2I_x)(2I_y)$	$4(2I_x)^{3/2}(2I_y)^{1/2}$
5	2300	normal	(-1, 0)	(2, 0)		$4(2I_x)^2$	
5	3002	normal	(3, -2)	(-2, 2)		$6(2I_x)(2I_y)$	
5	3011	normal	(3, 0)	(-2, 0)	(-3, 1)	$6(2I_x)(2I_y)$	$2(2I_x)^{3/2}(2I_y)^{1/2}$
5	3020	normal	(3, 2)	(-2, -2)	(-3, -1)	$6(2I_x)(2I_y)$	$4(2I_x)^{3/2}(2I_y)^{1/2}$
5	3200	normal	(1, 0)	(0, 0)		$6(2I_x)^2$	
5	4100	normal	(3, 0)	(-2, 0)		$8(2I_x)^2$	
5	5000	normal	(5, 0)	(-4, 0)		$10(2I_x)^2$	
5	0014	skew	(0, -3)		(0, 4)		$2(2I_y)^2$
5	0023	skew	(0, -1)		(0, 2)		$4(2I_y)^2$
5	0032	skew	(0, 1)		(0, 0)		$6(2I_y)^2$
5	0041	skew	(0, 3)		(0, -2)		$8(2I_y)^2$

B

B. Resonance Driving Terms

n	jklm	type	resonance	H-line	V-line	Amplitude H	Amplitude V
5	0050	skew	(0, 5)		(0, -4)		$10(2I_y)^2$
5	0212	skew	(-2, -1)		(2, 2)		$2(2I_x)(2I_y)$
5	0221	skew	(-2, 1)		(2, 0)		$4(2I_x)(2I_y)$
5	0230	skew	(-2, 3)		(2, -2)		$6(2I_x)(2I_y)$
5	0410	skew	(-4, 1)		(4, 0)		$2(2I_x)^2$
5	1103	skew	(0, -3)	(1, 3)		$2(2I_x)^{1/2}(2I_y)^{3/2}$	
5	1112	skew	(0, -1)	(1, 1)	(0, 2)	$2(2I_x)^{1/2}(2I_y)^{3/2}$	$2(2I_x)(2I_y)$
5	1121	skew	(0, 1)	(1, -1)	(0, 0)	$2(2I_x)^{1/2}(2I_y)^{3/2}$	$4(2I_x)(2I_y)$
5	1130	skew	(0, 3)	(1, -3)	(0, -2)	$2(2I_x)^{1/2}(2I_y)^{3/2}$	$6(2I_x)(2I_y)$
5	1301	skew	(-2, -1)	(3, 1)		$2(2I_x)^{3/2}(2I_y)^{1/2}$	
5	1310	skew	(-2, 1)	(3, -1)	(2, 0)	$2(2I_x)^{3/2}(2I_y)^{1/2}$	$2(2I_x)^2$
5	2003	skew	(2, -3)	(-1, 3)		$4(2I_x)^{1/2}(2I_y)^{3/2}$	
5	2012	skew	(2, -1)	(-1, 1)	(-2, 2)	$4(2I_x)^{1/2}(2I_y)^{3/2}$	$2(2I_x)(2I_y)$
5	2021	skew	(2, 1)	(-1, -1)	(-2, 0)	$4(2I_x)^{1/2}(2I_y)^{3/2}$	$4(2I_x)(2I_y)$
5	2030	skew	(2, 3)	(-1, -3)	(-2, -2)	$4(2I_x)^{1/2}(2I_y)^{3/2}$	$6(2I_x)(2I_y)$
5	2201	skew	(0, -1)	(1, 1)		$4(2I_x)^{3/2}(2I_y)^{1/2}$	
5	2210	skew	(0, 1)	(1, -1)	(0, 0)	$4(2I_x)^{3/2}(2I_y)^{1/2}$	$2(2I_x)^2$
5	3101	skew	(2, -1)	(-1, 1)		$6(2I_x)^{3/2}(2I_y)^{1/2}$	
5	3110	skew	(2, 1)	(-1, -1)	(-2, 0)	$6(2I_x)^{3/2}(2I_y)^{1/2}$	$2(2I_x)^2$
5	4001	skew	(4, -1)	(-3, 1)		$8(2I_x)^{3/2}(2I_y)^{1/2}$	
5	4010	skew	(4, 1)	(-3, -1)	(-4, 0)	$8(2I_x)^{3/2}(2I_y)^{1/2}$	$2(2I_x)^2$
6	0015	normal	(0, -4)		(0, 5)		$2(2I_y)^{5/2}$
6	0024	normal	(0, -2)		(0, 3)		$4(2I_y)^{5/2}$
6	0042	normal	(0, 2)		(0, -1)		$8(2I_y)^{5/2}$
6	0051	normal	(0, 4)		(0, -3)		$10(2I_y)^{5/2}$
6	0060	normal	(0, 6)		(0, -5)		$12(2I_y)^{5/2}$
6	0213	normal	(-2, -2)		(2, 3)		$2(2I_x)(2I_y)^{3/2}$
6	0222	normal	(-2, 0)		(2, 1)		$4(2I_x)(2I_y)^{3/2}$
6	0231	normal	(-2, 2)		(2, -1)		$6(2I_x)(2I_y)^{3/2}$

B.2. Amplitude, Resonances and Lines

n	jklm	type	resonance	H-line	V-line	Amplitude H	Amplitude V
6	0240	normal	(-2, 4)		(2, -3)		$8(2I_x)(2I_y)^{3/2}$
6	0411	normal	(-4, 0)		(4, 1)		$2(2I_x)^2(2I_y)^{1/2}$
6	0420	normal	(-4, 2)		(4, -1)		$4(2I_x)^2(2I_y)^{1/2}$
6	1104	normal	(0, -4)	(1, 4)		$2(2I_x)^{1/2}(2I_y)^2$	
6	1113	normal	(0, -2)	(1, 2)	(0, 3)	$2(2I_x)^{1/2}(2I_y)^2$	$2(2I_x)(2I_y)^{3/2}$
6	1131	normal	(0, 2)	(1, -2)	(0, -1)	$2(2I_x)^{1/2}(2I_y)^2$	$6(2I_x)(2I_y)^{3/2}$
6	1140	normal	(0, 4)	(1, -4)	(0, -3)	$2(2I_x)^{1/2}(2I_y)^2$	$8(2I_x)(2I_y)^{3/2}$
6	1302	normal	(-2, -2)	(3, 2)		$2(2I_x)^{3/2}(2I_y)$	
6	1311	normal	(-2, 0)	(3, 0)	(2, 1)	$2(2I_x)^{3/2}(2I_y)$	$2(2I_x)^2(2I_y)^{1/2}$
6	1320	normal	(-2, 2)	(3, -2)	(2, -1)	$2(2I_x)^{3/2}(2I_y)$	$4(2I_x)^2(2I_y)^{1/2}$
6	1500	normal	(-4, 0)	(5, 0)		$2(2I_x)^{5/2}$	
6	2004	normal	(2, -4)	(-1, 4)		$4(2I_x)^{1/2}(2I_y)^2$	
6	2013	normal	(2, -2)	(-1, 2)	(-2, 3)	$4(2I_x)^{1/2}(2I_y)^2$	$2(2I_x)(2I_y)^{3/2}$
6	2022	normal	(2, 0)	(-1, 0)	(-2, 1)	$4(2I_x)^{1/2}(2I_y)^2$	$4(2I_x)(2I_y)^{3/2}$
6	2031	normal	(2, 2)	(-1, -2)	(-2, -1)	$4(2I_x)^{1/2}(2I_y)^2$	$6(2I_x)(2I_y)^{3/2}$
6	2040	normal	(2, 4)	(-1, -4)	(-2, -3)	$4(2I_x)^{1/2}(2I_y)^2$	$8(2I_x)(2I_y)^{3/2}$
6	2202	normal	(0, -2)	(1, 2)		$4(2I_x)^{3/2}(2I_y)$	
6	2220	normal	(0, 2)	(1, -2)	(0, -1)	$4(2I_x)^{3/2}(2I_y)$	$4(2I_x)^2(2I_y)^{1/2}$
6	2400	normal	(-2, 0)	(3, 0)		$4(2I_x)^{5/2}$	
6	3102	normal	(2, -2)	(-1, 2)		$6(2I_x)^{3/2}(2I_y)$	
6	3111	normal	(2, 0)	(-1, 0)	(-2, 1)	$6(2I_x)^{3/2}(2I_y)$	$2(2I_x)^2(2I_y)^{1/2}$
6	3120	normal	(2, 2)	(-1, -2)	(-2, -1)	$6(2I_x)^{3/2}(2I_y)$	$4(2I_x)^2(2I_y)^{1/2}$
6	4002	normal	(4, -2)	(-3, 2)		$8(2I_x)^{3/2}(2I_y)$	
6	4011	normal	(4, 0)	(-3, 0)	(-4, 1)	$8(2I_x)^{3/2}(2I_y)$	$2(2I_x)^2(2I_y)^{1/2}$
6	4020	normal	(4, 2)	(-3, -2)	(-4, -1)	$8(2I_x)^{3/2}(2I_y)$	$4(2I_x)^2(2I_y)^{1/2}$
6	4200	normal	(2, 0)	(-1, 0)		$8(2I_x)^{5/2}$	
6	5100	normal	(4, 0)	(-3, 0)		$10(2I_x)^{5/2}$	
6	6000	normal	(6, 0)	(-5, 0)		$12(2I_x)^{5/2}$	
6	0114	skew	(-1, -3)		(1, 4)		$2(2I_x)^{1/2}(2I_y)^2$

B

B. Resonance Driving Terms

n	jklm	type	resonance	H-line	V-line	Amplitude H	Amplitude V
6	0123	skew	(-1, -1)		(1, 2)	$4(2I_x)^{1/2}(2I_y)^2$	
6	0132	skew	(-1, 1)		(1, 0)	$6(2I_x)^{1/2}(2I_y)^2$	
6	0141	skew	(-1, 3)		(1, -2)	$8(2I_x)^{1/2}(2I_y)^2$	
6	0150	skew	(-1, 5)		(1, -4)	$10(2I_x)^{1/2}(2I_y)^2$	
6	0312	skew	(-3, -1)		(3, 2)	$2(2I_x)^{3/2}(2I_y)$	
6	0321	skew	(-3, 1)		(3, 0)	$4(2I_x)^{3/2}(2I_y)$	
6	0330	skew	(-3, 3)		(3, -2)	$6(2I_x)^{3/2}(2I_y)$	
6	0510	skew	(-5, 1)		(5, 0)	$2(2I_x)^{5/2}$	
6	1005	skew	(1, -5)	(0, 5)		$2(2I_y)^{5/2}$	
6	1014	skew	(1, -3)	(0, 3)	(-1, 4)	$2(2I_y)^{5/2}$	$2(2I_x)^{1/2}(2I_y)^2$
6	1023	skew	(1, -1)	(0, 1)	(-1, 2)	$2(2I_y)^{5/2}$	$4(2I_x)^{1/2}(2I_y)^2$
6	1032	skew	(1, 1)	(0, -1)	(-1, 0)	$2(2I_y)^{5/2}$	$6(2I_x)^{1/2}(2I_y)^2$
6	1041	skew	(1, 3)	(0, -3)	(-1, -2)	$2(2I_y)^{5/2}$	$8(2I_x)^{1/2}(2I_y)^2$
6	1050	skew	(1, 5)	(0, -5)	(-1, -4)	$2(2I_y)^{5/2}$	$10(2I_x)^{1/2}(2I_y)^2$
6	1203	skew	(-1, -3)	(2, 3)		$2(2I_x)(2I_y)^{3/2}$	
6	1212	skew	(-1, -1)	(2, 1)	(1, 2)	$2(2I_x)(2I_y)^{3/2}$	$2(2I_x)^{3/2}(2I_y)$
6	1221	skew	(-1, 1)	(2, -1)	(1, 0)	$2(2I_x)(2I_y)^{3/2}$	$4(2I_x)^{3/2}(2I_y)$
6	1230	skew	(-1, 3)	(2, -3)	(1, -2)	$2(2I_x)(2I_y)^{3/2}$	$6(2I_x)^{3/2}(2I_y)$
6	1401	skew	(-3, -1)	(4, 1)		$2(2I_x)^2(2I_y)^{1/2}$	
6	1410	skew	(-3, 1)	(4, -1)	(3, 0)	$2(2I_x)^2(2I_y)^{1/2}$	$2(2I_x)^{5/2}$
6	2103	skew	(1, -3)	(0, 3)		$4(2I_x)(2I_y)^{3/2}$	
6	2112	skew	(1, -1)	(0, 1)	(-1, 2)	$4(2I_x)(2I_y)^{3/2}$	$2(2I_x)^{3/2}(2I_y)$
6	2121	skew	(1, 1)	(0, -1)	(-1, 0)	$4(2I_x)(2I_y)^{3/2}$	$4(2I_x)^{3/2}(2I_y)$
6	2130	skew	(1, 3)	(0, -3)	(-1, -2)	$4(2I_x)(2I_y)^{3/2}$	$6(2I_x)^{3/2}(2I_y)$
6	2301	skew	(-1, -1)	(2, 1)		$4(2I_x)^2(2I_y)^{1/2}$	
6	2310	skew	(-1, 1)	(2, -1)	(1, 0)	$4(2I_x)^2(2I_y)^{1/2}$	$2(2I_x)^{5/2}$
6	3003	skew	(3, -3)	(-2, 3)		$6(2I_x)(2I_y)^{3/2}$	
6	3012	skew	(3, -1)	(-2, 1)	(-3, 2)	$6(2I_x)(2I_y)^{3/2}$	$2(2I_x)^{3/2}(2I_y)$
6	3021	skew	(3, 1)	(-2, -1)	(-3, 0)	$6(2I_x)(2I_y)^{3/2}$	$4(2I_x)^{3/2}(2I_y)$

B.2. Amplitude, Resonances and Lines

n	jklm	type	resonance	H-line	V-line	Amplitude H	Amplitude V
6	3030	skew	(3, 3)	(-2, -3)	(-3, -2)	$6(2I_x)(2I_y)^{3/2}$	$6(2I_x)^{3/2}(2I_y)$
6	3201	skew	(1, -1)	(0, 1)		$6(2I_x)^2(2I_y)^{1/2}$	
6	3210	skew	(1, 1)	(0, -1)	(-1, 0)	$6(2I_x)^2(2I_y)^{1/2}$	$2(2I_x)^{5/2}$
6	4101	skew	(3, -1)	(-2, 1)		$8(2I_x)^2(2I_y)^{1/2}$	
6	4110	skew	(3, 1)	(-2, -1)	(-3, 0)	$8(2I_x)^2(2I_y)^{1/2}$	$2(2I_x)^{5/2}$
6	5001	skew	(5, -1)	(-4, 1)		$10(2I_x)^2(2I_y)^{1/2}$	
6	5010	skew	(5, 1)	(-4, -1)	(-5, 0)	$10(2I_x)^2(2I_y)^{1/2}$	$2(2I_x)^{5/2}$

Bibliography

- [1] *CERN Resources Website*. URL: <https://home.cern/resources> (visited on 10/02/2023).
- [2] Joschua Dilly. “Corrections of High-Order Nonlinear Errors in the LHC and HL-LHC Beam Optics”. To Be Submitted. Humboldt University of Berlin, 2022.
- [3] Rob Wolf. *Engineering Specification: Field Error Naming Conventions for LHC Magnets*. Tech. rep. LHC-M-ES-001.00. CERN, Oct. 2001. URL: <https://lhc-div-mms.web.cern.ch/lhc-div-mms/tests/MAG/FiDeL/Documentation/lhc-m-es-0001-30-00.pdf> (visited on 02/11/2019).
- [4] Keintzel Jacqueline. “Beam Optics Design, Measurement and Correction Strategies for Circular Colliders at the Energy and Luminosity Frontier”. en. PhD thesis.
- [5] Rogelio Tomás. “Direct Measurement of Resonance Driving Terms in the Super Proton Synchrotron (SPS) of CERN Using Beam Position Monitors”. PhD Thesis. 2003. URL: <http://cds.cern.ch/record/615164> (visited on 03/07/2018).
- [6] Andrea Franchi. “Studies and Measurements of Linear Coupling and Nonlinearities in Hadron Circular Accelerators”. Doctoral Thesis. Johann Wolfgang Goethe-Universität, Sept. 2006. URL: <https://publikationen.ub.uni-frankfurt.de/frontdoor/index/index/year/2006/docId/2270> (visited on 01/19/2018).

Bibliography

- [7] E. D Courant and H. S Snyder. “Theory of the Alternating-Gradient Synchrotron”. In: *Annals of Physics* 3.1 (Jan. 1958), pp. 1–48. DOI: [10.1016/0003-4916\(58\)90012-5](https://doi.org/10.1016/0003-4916(58)90012-5). URL: <http://www.sciencedirect.com/science/article/pii/0003491658900125> (visited on 05/09/2019).
- [8] A J Dragt. “An Overview of Lie Methods for Accelerator Physics”. en. In: *Proceedings of PAC*. Pasadena, CA USA: JACoW, 2013.
- [9] Ghislain J Roy. “Analysis of the optics of the Final Focus Test Beam using Lie algebra based techniques”. en. PhD thesis. 1992.
- [10] Félix Simon Carlier. “A Nonlinear Future: Measurements and Corrections of Nonlinear Beam Dynamics Using Forced Transverse Oscillations”. ISBN: 9789464022148. PhD Thesis. 2020. URL: <http://cds.cern.ch/record/2715765/>.
- [11] Jacqueline Keintzel et al. “Second-Order Dispersion Measurement in LHC”. In: *IPAC’19*. Melbourne, Australia, 2019, MOPMP027. DOI: [10.18429/JACoW-IPAC2019-MOPMP027](https://doi.org/10.18429/JACoW-IPAC2019-MOPMP027).
- [12] Joschua Dilly and Mael Le Garrec. *On the derivation of Amplitude Detuning and Chromaticity Formulas for Particle Accelerators*. en. arXiv:2301.09132 [physics]. Jan. 2023. URL: <http://arxiv.org/abs/2301.09132> (visited on 01/24/2023).
- [13] M. Wendt. “BPM Systems: A Brief Introduction to Beam Position Monitoring”. In: *ArXiv200514081 Phys.* (May 2020). arXiv: 2005.14081. URL: <http://arxiv.org/abs/2005.14081> (visited on 09/01/2021).
- [14] A. Nosych. *Geometrical Non-Linearity Correction Procedure Of LHC Beam Position Monitors*. 2014. URL: <https://edms.cern.ch/document/1342295/1>.
- [15] R. Miyamoto et al. “Parametrization of the driven betatron oscillation”. en. In: *Physical Review Special Topics - Accelerators and Beams* 11.8 (Aug. 2008), p. 084002. DOI: [10.1103/PhysRevSTAB.11.084002](https://doi.org/10.1103/PhysRevSTAB.11.084002). URL: <https://link.aps.org/doi/10.1103/PhysRevSTAB.11.084002>.

Bibliography

- [16] Javier Serrano and Matthieu Cattin. *The LHC AC Dipole system: an introduction.* en. 2010.
- [17] M. Le Garrec. *Non-linear Chromaticity GUI*. Oct. 2022. URL: <https://gitlab.cern.ch/mlegarre/nl-chroma-gui>.
- [18] Ewen Hamish Maclean et al. *Commissioning of the nonlinear chromaticity at injection for LHC Run II*. eng. Accelerators & Technology Sector Note 2016-0013. Issue: 2016-0013. 2016. URL: <https://cds.cern.ch/record/2121333>.
- [19] E H Maclean et al. “Non-linear Chromaticity Studies of the LHC at Injection”. en. In: *Proc. IPAC’11*. WEPC078. San Sebastian, Spain, Sep. 2011: JACoW Publishing, Geneva, Switzerland, 2011, pp. 2199–2201. URL: <https://jacow.org/IPAC2011/papers/WEPC078.pdf>.
- [20] Ewen Hamish Maclean, Felix Simon Carlier, and Jaime Coello de Portugal. “Commissioning of Non-linear Optics in the LHC at Injection Energy”. In: *Proc. IPAC*. Busan, Korea, 2016, p. 4. DOI: [10.18429/JACoW-IPAC2016-THPMR039](https://doi.org/10.18429/JACoW-IPAC2016-THPMR039). URL: <https://cds.cern.ch/record/2207446>.
- [21] Ewen Hamish Maclean et al. “Measurement of Nonlinear Observables in the Large Hadron Collider Using Kicked Beams”. In: *Phys. Rev. ST Accel. Beams* 17.8 (Aug. 2014), p. 081002. DOI: [10.1103/PhysRevSTAB.17.081002](https://doi.org/10.1103/PhysRevSTAB.17.081002). URL: <https://link.aps.org/doi/10.1103/PhysRevSTAB.17.081002> (visited on 03/07/2018).
- [22] Ewen Hamish Maclean et al. “Measurement of nonlinear observables in the Large Hadron Collider using kicked beams”. In: *Physical Review Special Topics - Accelerators and Beams* 17.8 (Aug. 2014). Number: 8, p. 081002. DOI: [10.1103/PhysRevSTAB.17.081002](https://doi.org/10.1103/PhysRevSTAB.17.081002). URL: <https://link.aps.org/doi/10.1103/PhysRevSTAB.17.081002> (visited on 03/07/2018).
- [23] M. Gasior and R. Jones. *The Principle and First Results of Betatron Tune Measurement by Direct Diode Detection*. 2005. URL: <http://cds.cern.ch/record/883298>.

Bibliography

- [24] A. Boccardi et al. *First Results from the LHC BBQ Tune and Chromaticity Systems*. 2009. URL: <http://cds.cern.ch/record/1156349/>.
- [25] P. Hagen et al. *Wise: An adaptive simulation of the LHC optics*. Tech. rep. 2006. URL: <https://cds.cern.ch/record/977794/files/lhc-project-report-971.pdf>.
- [26] Tobias Persson et al. “Optics Measurements and Correction Plans for the HL-LHC”. In: *IPAC'21*. ISSN: 2673-5490. Campinas, Brazil: JACOW Publishing, Geneva, Switzerland, Aug. 2021, pp. 2656–2659. doi: [10.18429/JACoW-IPAC2021-WEPAB026](https://doi.org/10.18429/JACoW-IPAC2021-WEPAB026). URL: <https://accelconf.web.cern.ch/ipac2021/doi/JACoW-IPAC2021-WEPAB026.html> (visited on 11/29/2021).

List of Publications

Journal Publications

Journal Publications (co-author)

Conference Proceedings

Conference Proceedings (co-author)

- (1) Tobias Persson et al. “Optics Measurements and Correction Plans for the HL-LHC”. in: *IPAC’21*. ISSN: 2673-5490. Campinas, Brazil: JACOW Publishing, Geneva, Switzerland, Aug. 2021, pp. 2656–2659. DOI: [10.18429 / JACoW-IPAC2021-WEPAB026](https://doi.org/10.18429/JACoW-IPAC2021-WEPAB026). URL: <https://accelconf.web.cern.ch/ipac2021/doi/JACoW-IPAC2021-WEPAB026.html> (visited on 11/29/2021)

Notes